REPORT 1056

THEORETICAL ANTISYMMETRIC SPAN LOADING FOR WINGS OF ARBITRARY PLAN FORM AT SUBSONIC SPEEDS [1]

By JOHN DEYOUNG

SUMMARY

A simplified lifting-surface theory that includes effects of compressibility and spanwise variation of section lift-curve slope is used to provide charts with which antisymmetric loading due to arbitrary antisymmetric angle of attack can be found for wings having symmetric plan forms with a constant spanwise sweep angle of the quarter-chord line. Consideration is given to the flexible wing in roll. Aerodynamic characteristics due to rolling, deflected ailerons, and sideslip of wings with dihedral are considered. Solutions are presented for straight-tapered wings for a range of swept plan forms.

INTRODUCTION

Reference 1 has been for many years the standard reference for estimating the stability and control characteristics of wings. The lifting-line theory on which this work was based gave generally satisfactory results for straight wings having the aspect ratios considered; however, the use of wing sweep combined with low aspect ratio has made an extension of this work desirable. Lifting-line theory cannot adequately account for the increased induction effects due to sweep and low aspect ratio; consequently, it has been found necessary to turn to the more complex lifting-surface theories.

Of the many possible procedures, a simplified lifting-surface theory proposed by Weissinger and further developed and extended in reference 2 has been found especially suited to the rapid computation of characteristics of wings of arbitrary plan form. Comparisons with experiment have generally verified the theoretical predictions. In reference 2, this method has been used to compute for plain, unflapped wings, the aerodynamic characteristics dependent on symmetric loading. The same simplified lifting-surface theory can be extended to predict the span loading resulting from antisymmetric [2] distribution of the wing angle of attack. From such loadings the damping moment due to rolling, the rolling moment due to deflected ailerons, and the rolling moment due to dihedral angle with the wing in sideslip can be determined. A recent publication (reference 3) makes use of the simplified lifting-surface theory to find span-loading characteristics of straight-tapered swept wings in roll and loading due to dihedral angle with the wing in sideslip. Experimental checks of the theory for the damping-in-roll coefficient and rolling moment due to sideslip were very favorable. The range of plan forms considered in reference 3 is somewhat limited and aileron effectiveness was not included. The loading due to aileron deflection normally involves excessive labor when computed by means of the simplified lifting-surface theory; however, development of the theory, presented in reference 4, that deals with flap and aileron effectiveness for low-aspect-ratio wings provides a means by which the simplified lifting-surface method can be used to obtain spanwise loading due to aileron deflection.

It is the purpose of the present analysis to provide simple methods of finding antisymmetric loading and the associated aerodynamic coefficients and derivatives for wings with symmetric plan forms limited only by a straight quarter-chord line over the semispan. Means will be presented for finding quickly the aerodynamic coefficients of span loading due to rolling, of span loading due to deflected ailerons, and of span loading due to sideslip of wings with dihedral. Flexible wings, when the flexure depends principally on span loading as in loading due to rolling, can be included in the analysis.

NOTATION

A	aspect ratio $\left(\frac{b^2}{S}\right)$
b	wing span measured perpendicular to the plane of symmetry, feet
c	wing chord, feet [3]
c_a	aileron chord, feet [3]
c_{av}	mean wing chord $\left(\frac{S}{b}\right)$, feet [3]
c_l	local lift coefficient $\left(\frac{\text{local lift}}{qc}\right)$
C_{D_i}	induced drag coefficient $\left(\frac{\text{induced drag}}{qS}\right)$
C_l	rolling-moment coefficient $\left(\frac{\text{rolling moment}}{qSb}\right)$
C_{l_p}	rolling moment due to rolling $\left[\frac{\partial C_l}{\partial(pb/2V)}\right]$, per radian
C_{l_δ}	rolling moment due to aileron deflection $\left(\frac{\partial C_l}{\partial \delta}\right)$, per radian
$\frac{c_l c}{C_l c_{av}}$	spanwise loading coefficient for unit rolling moment $\left(\frac{2AG}{C_l}\right)$
d_r	scale factor

[1] Supersedes NACA TN 2140, "Theoretical Antisymmetric Span Loading for Wings of Arbitrary Plan Form at Subsonic Speeds" by John DeYoung, 1950.
[2] The word "antisymmetric" is understood to indicate that a distribution of loading or angle of attack is equal in absolute magnitude on each half of the wing but of opposite sign.
[3] Measured parallel to the plane of symmetry.

e_{nk} factors of loading interpolation function

G spanwise loading coefficient or dimensionless circulation $\left(\frac{c_l c}{2b}\right)$ or $\left(\frac{\Gamma_c}{bV}\right)$

$\overline{G}$ spanwise loading coefficient due to rolling $\left(\frac{G}{pb/2V}\right)$, per radian

$\overline{\overline{G}}$ spanwise loading coefficient due to aileron deflection $\left(\frac{G}{\delta}\right)$, per radian

H_ν wing geometry, compressibility, and section lift-curve-slope parameter $\left[d_\nu\left(\frac{1}{\kappa_\nu}\right)\left(\frac{b}{c_\nu/\beta}\right)\right]$

h_n integration factors for spanwise loading due to ailerons

M Mach number

m arbitrary number of span stations defined by $\eta=\cos\frac{n\pi}{m+1}$

p rate of rolling, radians per second

$pb/2V$ wing-tip helix angle, radians

$p_{\nu n}$ coefficient depending on wing geometry and indicating the influence of antisymmetric loading at span station n on the downwash angle at span station ν

q free-stream dynamic pressure, pounds per square foot

S wing area, square feet

t ratio of aileron chord to wing chord [3] $\left(\frac{c_a}{c}\right)$

V free-stream velocity, feet per second

w induced velocity, normal to the lifting surface, positive for downwash, feet per second

y lateral coordinate measured from the wing root perpendicular to the plane of symmetry, feet

α_ν section angle of attack at span station ν, radians [3]

$\Delta\alpha_\nu$ angle of antisymmetric twist of the elastic wing produced by the loading due to rolling, radians [3]

$\frac{d\alpha}{d\delta}$ rate of change of wing-section angle of attack with control-surface angle for constant section lift coefficient [3]

β compressibility parameter $(\sqrt{|1-M^2|})$

$\overline{\beta}$ angle of sideslip, radians

Γ dihedral angle measured perpendicular to the plane of symmetry, radians

Γ_c spanwise circulation, feet squared per second

δ angle of deflection of full wing-chord control surface, radians [3]

$\underline{\delta}$ angle of deflection of full-wing-chord control surface, measured perpendicular to the hinge line, radians

η dimensionless lateral coordinate $\left(\frac{y}{b/2}\right)$

η_a dimensionless aileron span $\left(\frac{\text{aileron span}}{b/2}\right)$

$\eta_{c.p.}$ spanwise center of pressure on one wing panel $\left(\frac{y_{c.p.}}{b/2}\right)$

θ trigonometric spanwise coordinate ϕ, indicating the edge of the aileron span, radians

κ_ν ratio of section lift-curve slope at a span station ν to $\frac{2\pi}{\beta}$, both at the same Mach number

Λ sweep angle of the wing quarter-chord line, positive for sweepback, degrees

Λ_β compressibility sweep-angle parameter $\left[\tan^{-1}\left(\frac{\tan\Lambda}{\beta}\right)\right]$, degrees

λ taper ratio $\left(\frac{\text{tip chord}}{\text{root chord}}\right)$

ϕ trigonometric spanwise coordinate $(\cos^{-1}\eta)$, radians

SUBSCRIPTS

n, ν integers pertaining to specific span stations given by $\eta=\cos\frac{n\pi}{8}$ or $\eta=\cos\frac{\nu\pi}{8}$

k pertaining to span station k

$c.\ p.$ center of pressure

a aileron

t pertaining to fraction-of-wing-chord ailerons

T wing tip

R wing root

av average or mean

DEVELOPMENT OF METHOD

The simplified lifting-surface method used herein replaces a lifting surface by a lifting vortex located at the wing one-quarter-chord line. The boundary condition for determining the vortex strength distribution specifies that, along the three-quarter-chord line of the wing, there shall be no flow through the lifting surface. In effect, this specifies that, at the three-quarter-chord line, the ratio of the velocity normal to the mean camber line (induced by the bound and trailing vortices) to the velocity of the free stream shall equal the sine of the angle of attack.

Span loadings are theoretically additive. Since the symmetric angle-of-attack distribution contributes only to symmetric loading, it follows that the antisymmetric loading is independent of symmetrically distributed wing twist or camber; hence, to find antisymmetric loading, it is only necessary to consider the loading resulting form the antisymmetric distribution of the angle of attack across the wing span. In the subject case, such a distribution is experienced by the wing as induced angle due to rolling,[4] the effective twist due to aileron deflection, or sideslip of the wing with dihedral.

[3] Measured parallel to the plane of symmetry.

[4] In considering the case of the angle induced by rolling as equivalent to an antisymmetric distribution of twist, it must be noted that account should be taken of the fact that a rolling wing leaves a twisted vortex trail; whereas a twisted wing does not. The difference in induction effects on the wing of the straight and twisted vortex is considered insignificant here, as has been assumed in other analyses.

For an antisymmetric angle-of-attack distribution, the loading distribution will be equal in absolute magnitude on each semispan, but of opposite sign. The loading therefore needs only to be found over the semispan, and, since the loading is zero at the wing root, only span stations outboard need be considered. The mathematical development of the simplified lifting-surface method for the case of antisymmetric loading is given in appendix A. As shown in appendix A, $(m-1)/2$ linear equations in terms of loading distribution are obtained which satisfy the wing angle-of-attack conditions [5] at the three-quarter-chord line at m stations n, where m is an arbitrary odd integer. These equations are represented by the summations

$$\alpha_\nu=\sum_{n=1}^{\frac{m-1}{2}} p_{\nu n}G_n, \quad \nu=1,2,3,\ldots\frac{m-1}{2} \tag{1}$$

where

α_ν antisymmetric angle of attack at wing station ν

$p_{\nu n}$ coefficients that for a given value of m depend on wing geometry, compressibility, and section lift-curve slope

G_n loading coefficients at span stations n

The application in appendix A of the present report is with $m=7$. Since the loading at the midspan station is known to be zero, consideration is required of only three stations: $n=1$, 2, 3, equal to wing semispan positions of $\eta=\cos(n\pi/8)=0.924$; 0.707; and 0.383. Equation (1) thus becomes

$$\alpha_\nu=\sum_{n=1}^{3} p_{\nu n}G_n, \qquad \nu=1,2,3 \tag{2}$$

where the integer ν pertains to span station $\eta=\cos(\nu\pi/8)$

To obtain the loading coefficients $G_n=(c_l c/2b)_n$, it remains only to evaluate the coefficients $p_{\nu n}$ and the spanwise variation of the antisymmetric angle of attack α_ν.

EVALUATION OF COEFFICIENTS $p_{\nu n}$

Since m is chosen, $p_{\nu n}$ becomes a function only of wing geometry, compressibility, and section lift-curve slope. The effects of compressibility and section lift-curve slope are equivalent to a change in wing plan form [6] and can be accounted for by a proper adjustment of the $p_{\nu n}$ values. As shown in appendix B, $p_{\nu n}$ can be conveniently presented as a function of two parameters, namely, a compressible-sweep-angle parameter defined as $\Lambda_\beta=\tan^{-1}(\tan\Lambda/\beta)$ and a parameter H_ν involving the ratio of wing span to wing chord and variable section lift-curve slope, defined by

$$H_\nu=d_\nu\left(\frac{1}{\kappa_\nu}\right)\left(\frac{b}{c_\nu/\beta}\right) \tag{3}$$

where

κ_ν ratio of experimental section lift-curve slope at span station ν to the theoretical value of $2\pi/\beta$, both at the same Mach number

c_ν wing chord at span station ν

The value d_ν is a scale factor given by

$$\left.\begin{aligned} d_\nu&=0.061 \text{ for } \nu=1\\ &=0.234 \text{ for } \nu=2\\ &=0.381 \text{ for } \nu=3\end{aligned}\right\} \tag{4}$$

Equation (3) can be written in alternative form that gives H_ν in terms of wing geometry parameters that are more significant; thus

$$H_\nu=d_\nu\left(\frac{\beta A}{\kappa_{av}}\right)\left[\frac{1}{(\kappa_\nu/\kappa_{av})(c_\nu/c_{av})}\right] \tag{5}$$

where

κ_{av} ratio of average section lift-curve slope to $2\pi/\beta$ both at the same Mach number

κ_ν/κ_{av} spanwise distribution of section lift-curve slope for a given Mach number

c_ν/c_{av} spanwise distribution of the wing chord

$(\beta A/\kappa_{av})$ compressible aspect ratio and average section lift-curve-slope parameter

The term $\dfrac{1}{(\kappa_\nu/\kappa_{av})(c_\nu/c_{av})}$ of equation (5) gives an effective aerodynamic taper of a wing. The distribution of κ_ν/κ_{av} may vary with Mach number, particularly at transonic speeds (e. g., due to spanwise variation of airfoil section). However, since the distribution contributes to taper effect, the loading distribution and not the total loading will be appreciably affected.

With H_ν determined from equations (3) or (5) and (4), the values of $p_{\nu n}$, nine in all, are presented in figure 1 where $p_{\nu n}$ is given as a function of H_ν for various values of Λ_β.

[5] The reader should note that the boundary condition is given by $w_\nu=V\sin\alpha_\nu$ from which $(w/V)_\nu$ is seen to equal $\sin\alpha_\nu$. The substitution of α_ν for $\sin\alpha_\nu$ has the effect of increasing the value of loading on the wing above that necessary to satisfy the boundary condition. However, the boundary condition was fixed assuming that the shed vortices moved downstream in the extended chord plane. A more realistic picture is obtained if the vortices are assumed to move downstream in a horizontal plane from the wing trailing edge. It can be seen readily that, if this occurs, the normal component of velocity induced by the trails at the three-quarter-chord line is reduced and, if the boundary condition is to continue to be satisfied, the strength of the bound vortex must increase. It follows that substitution of α_ν for $\sin\alpha_\nu$ then has the effect of accounting for the bending up of the trailing vortices. It is not known how exact the correction is, but the calculations and experimental verification show it to be of the correct order.

[6] Compressibility and section lift-curve slope are discussed in the section "Discussion" and in the appendix B.

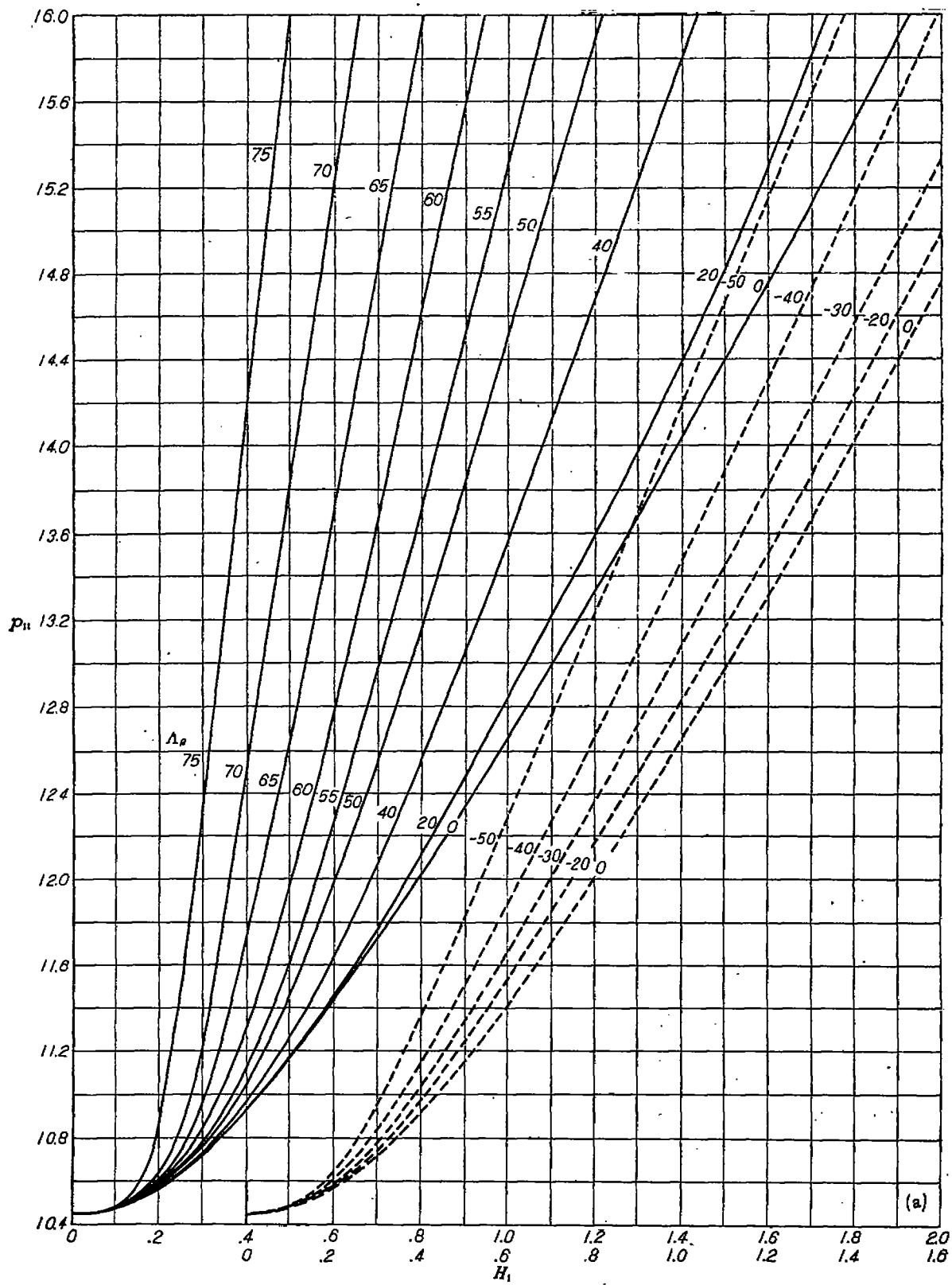

(a) $\nu=1$, $n=1$, $d_1=0.061$.

FIGURE 1.—Influence coefficients, $p_{\nu n}$, for antisymmetric spanwise loading plotted as a function of the wing geometric parameter, H_ν, for values of the compressible sweep parameter, Λ_β degrees.

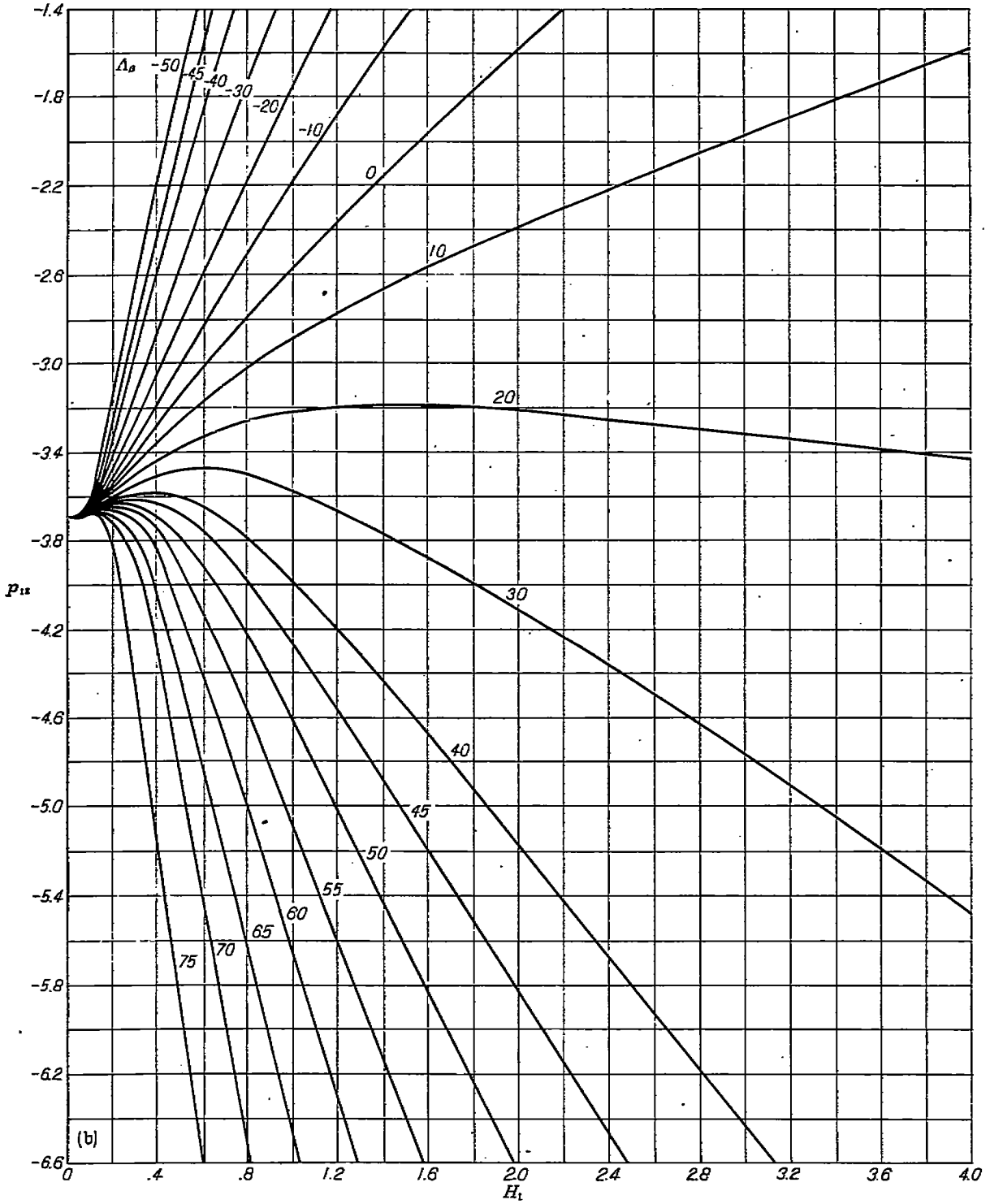

(b) $\nu=1$, $n=2$, $d_1=0.061$.

FIGURE 1.—Continued.

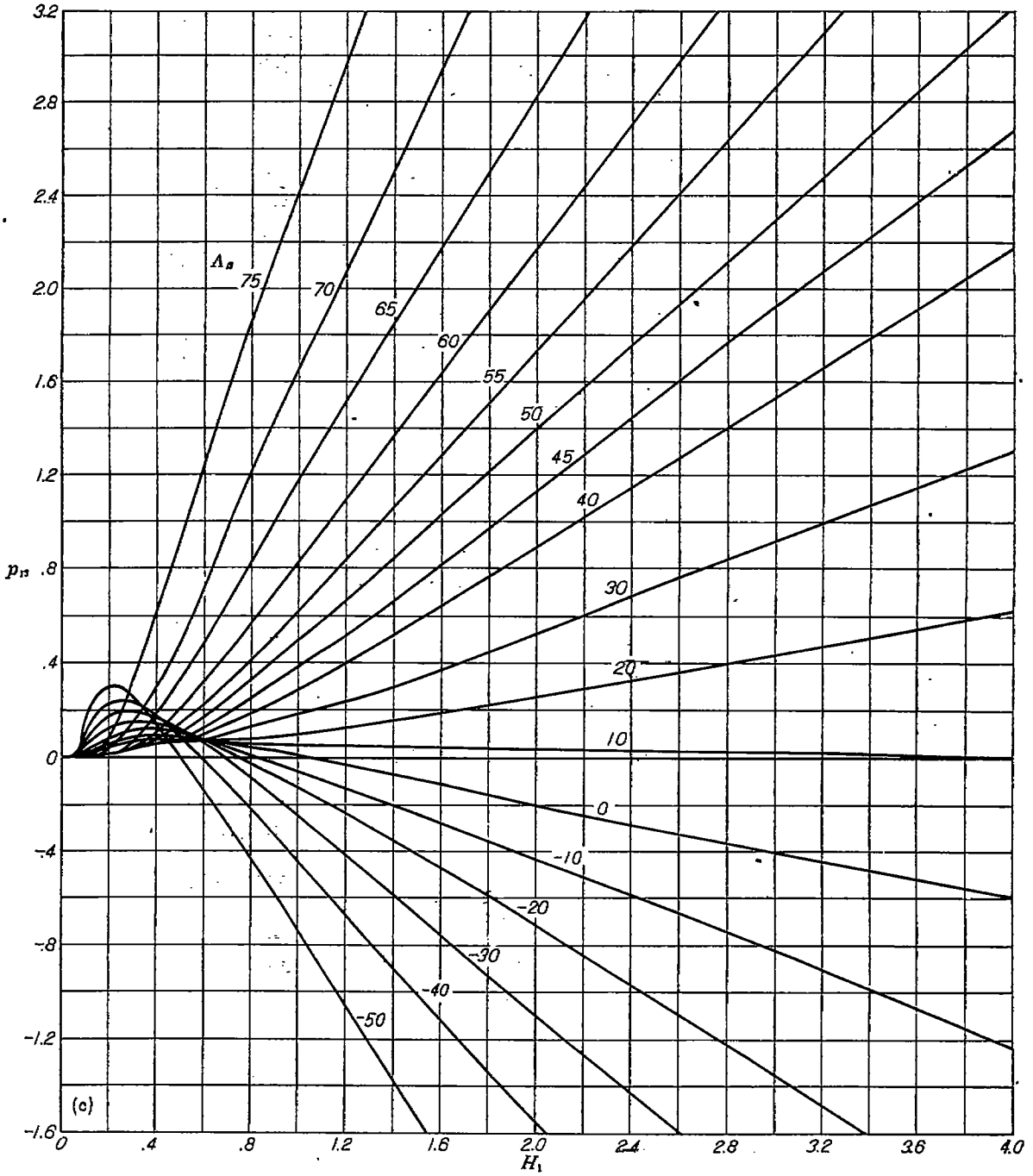

(c) $r=1$, $\eta=3$, $d_1=0.061$.

FIGURE 1.—Continued.

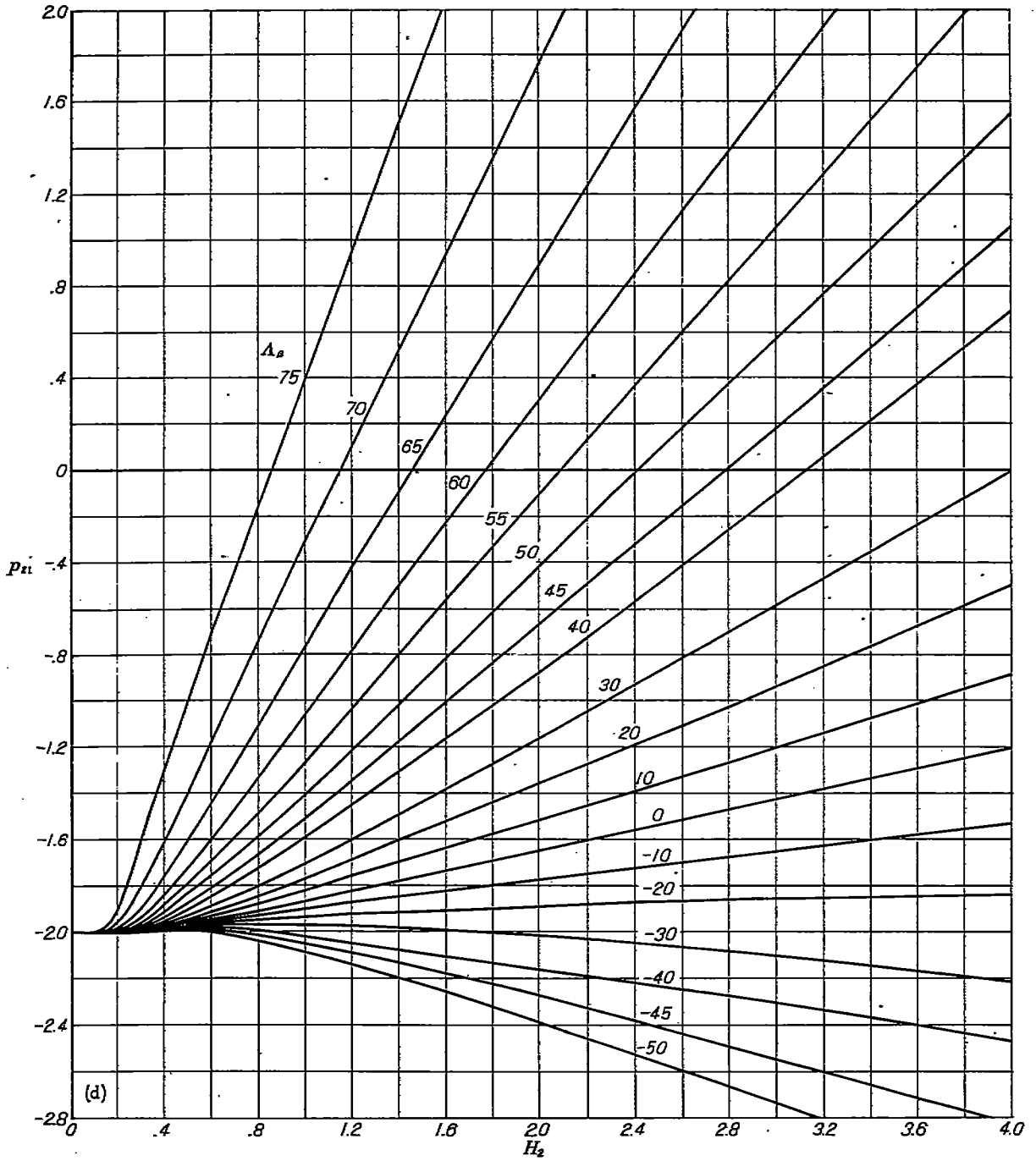

(d) $\nu=2$, $n=1$, $d_1=0.284$.

FIGURE 1.—Continued.

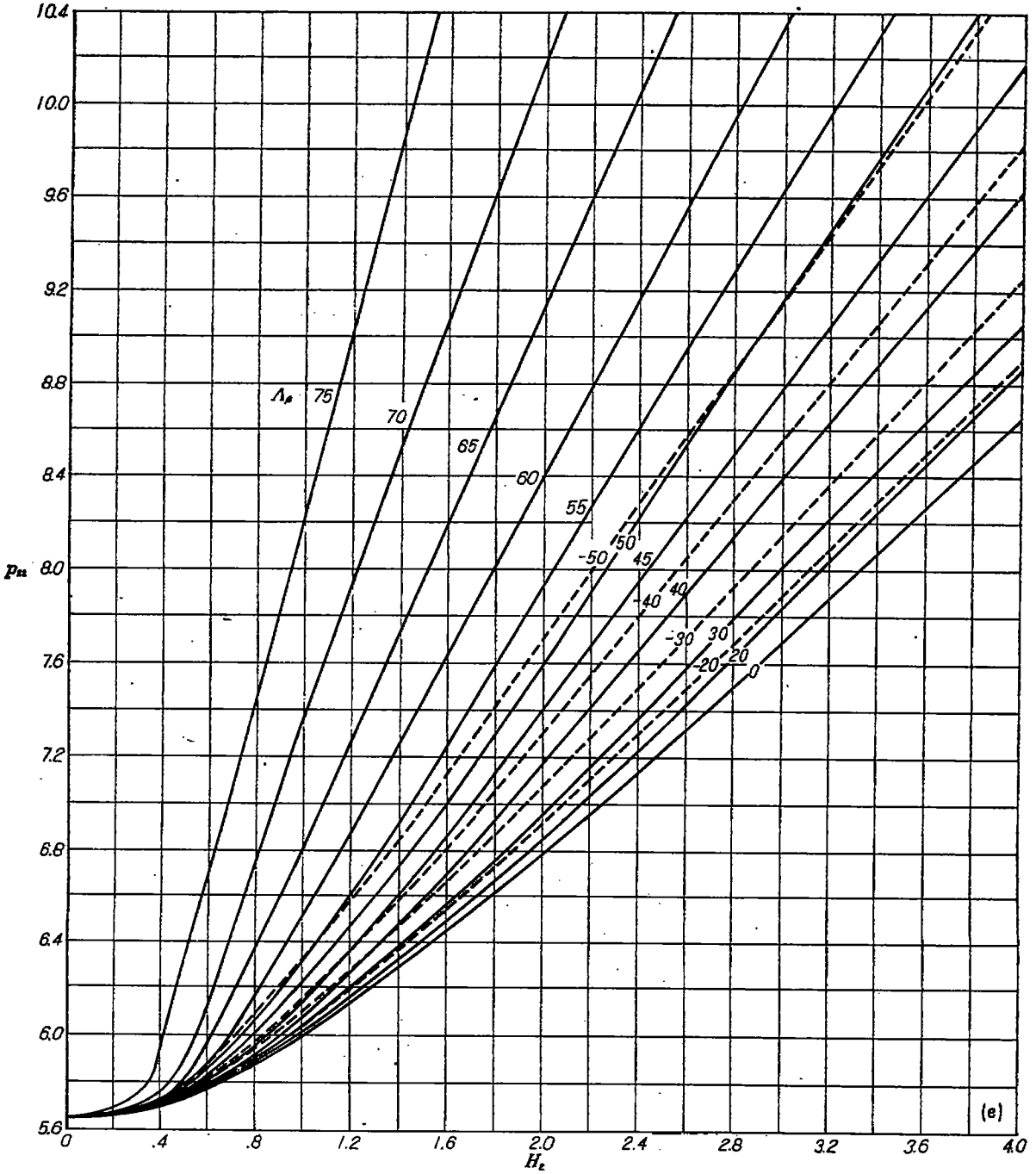

(e) $\nu=2$, $n=2$, $d_2=0.234$.

FIGURE 1.—Continued.

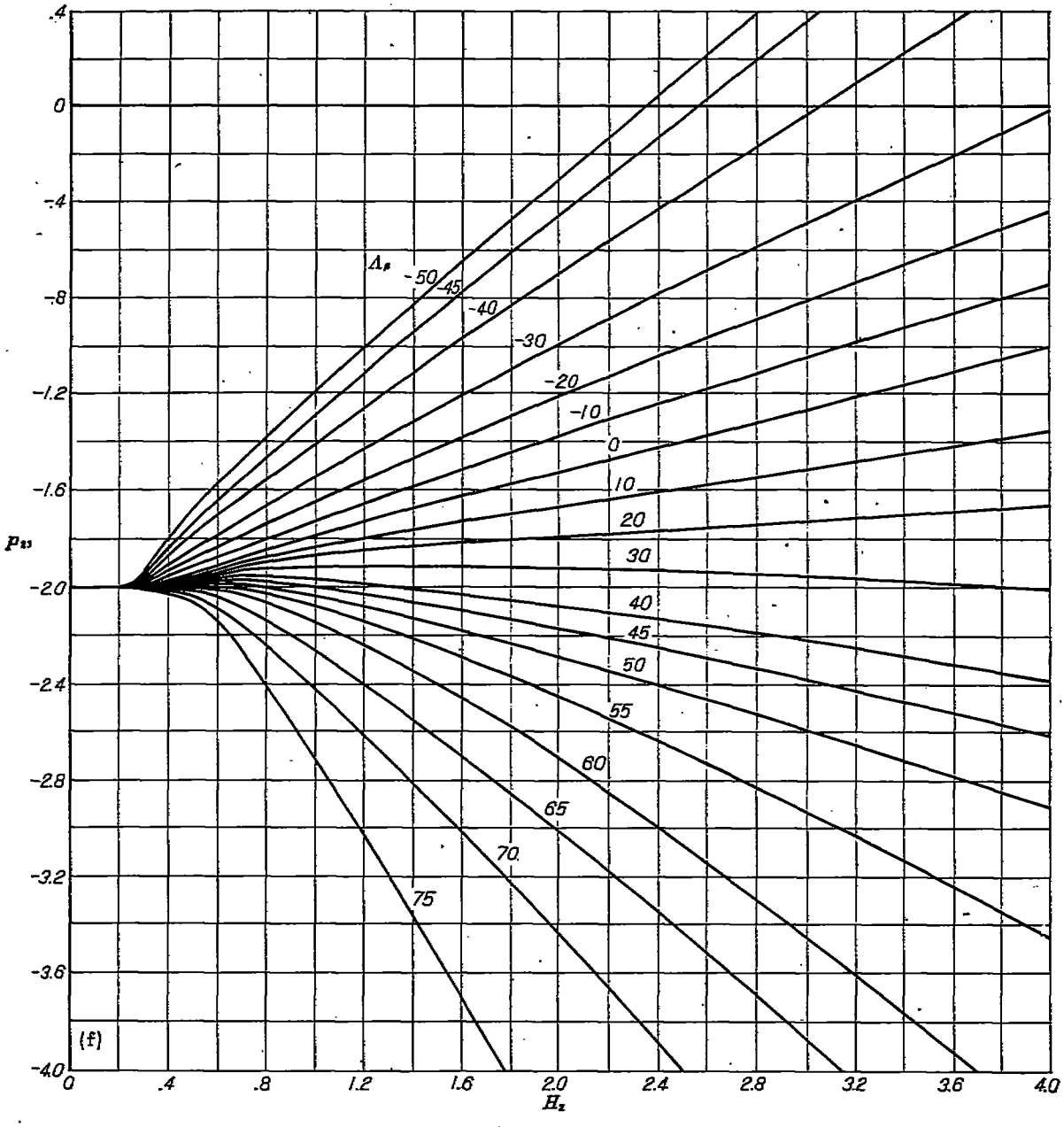

(f) $r=2$, $n=3$, $d_2=0.234$.

FIGURE 1.—Continued.

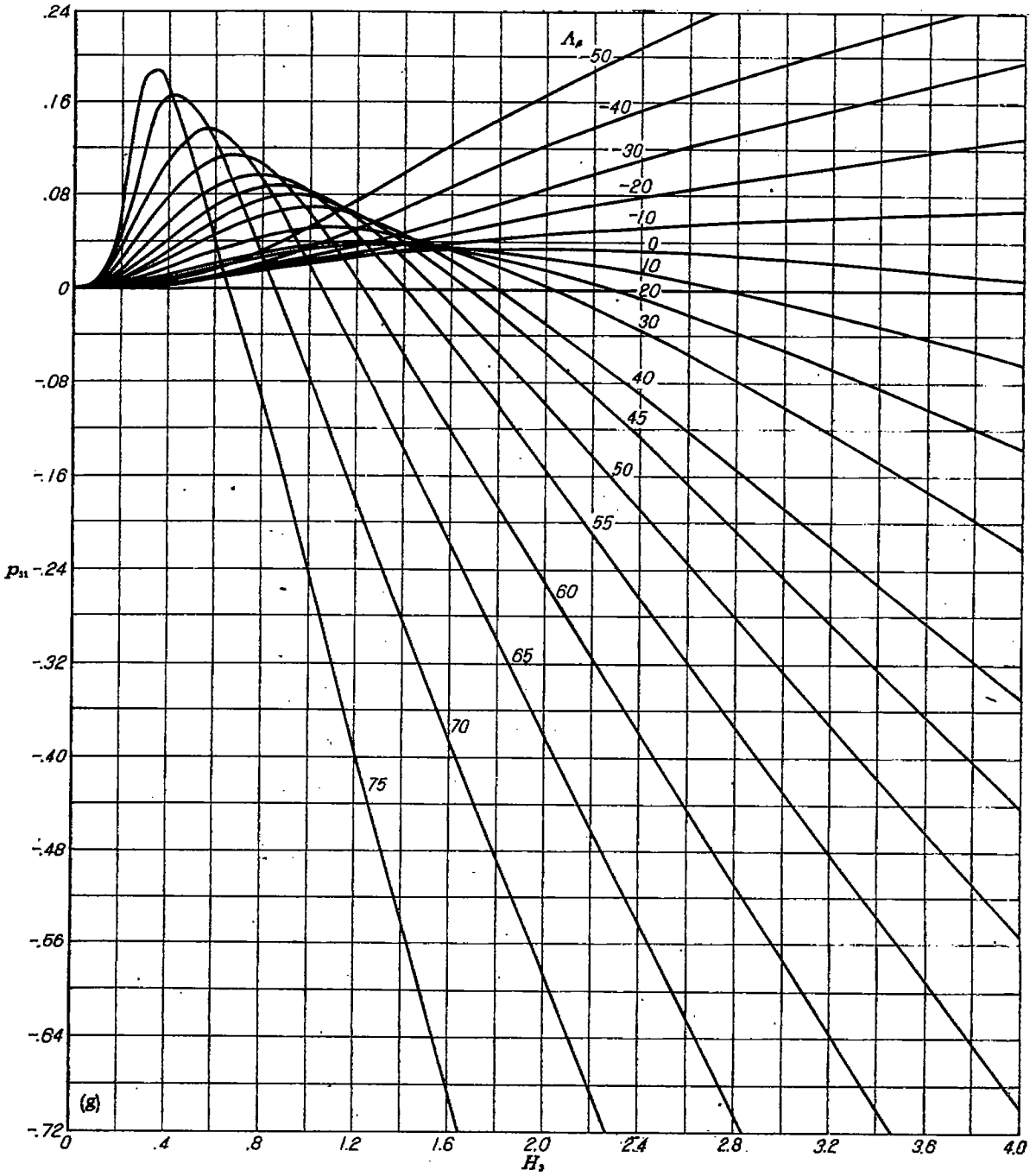

(g) $r=3$, $n=1$, $d_3=0.381$.

FIGURE 1.—Continued.

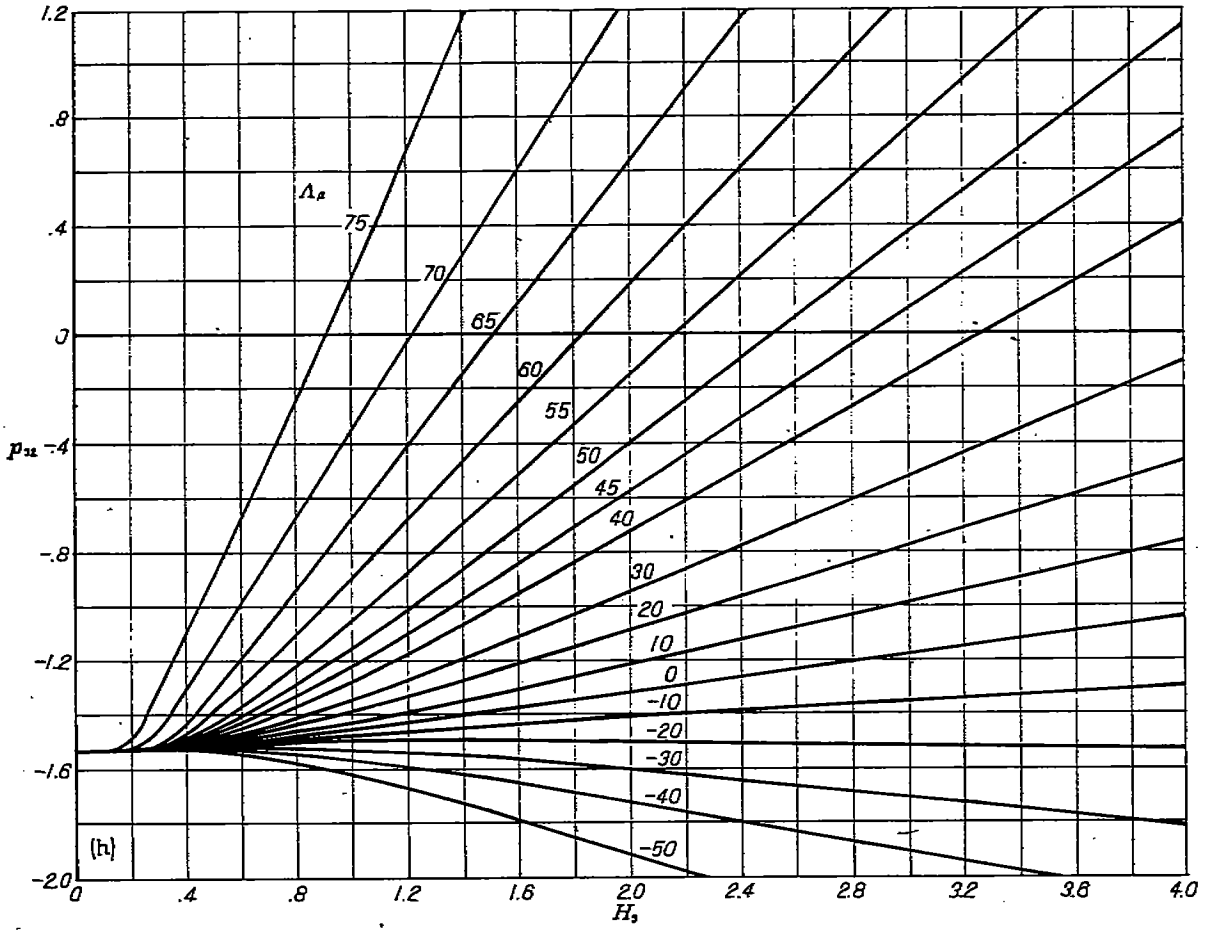

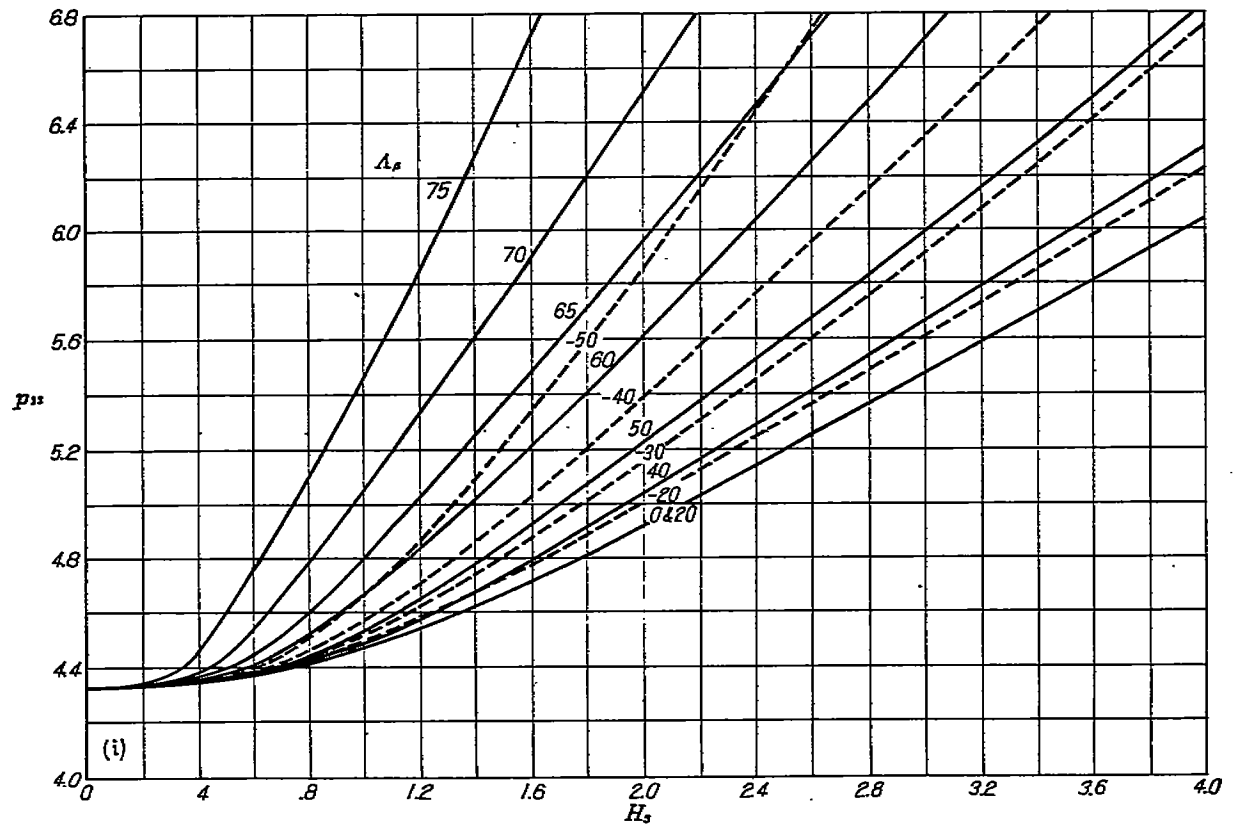

(h) $\nu=3$, $n=2$, $d_3=0.381$;
(i) $\nu=3$, $n=3$, $d_3=0.381$.

FIGURE 1.—Concluded.

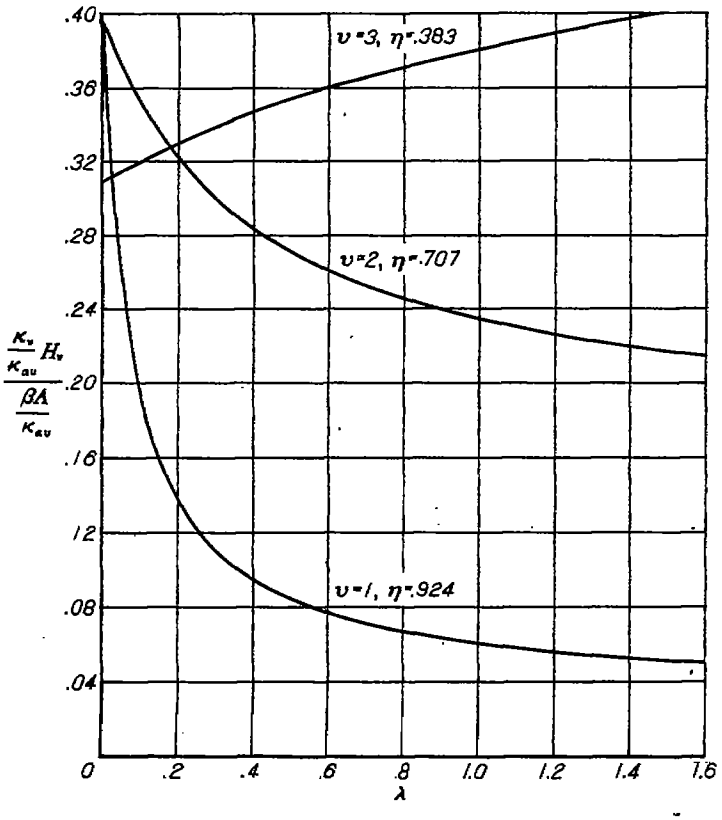

FIGURE 2.—Variation of the geometric parameter $\frac{\frac{\kappa_\nu}{\kappa_{a\nu}} H_\nu}{\frac{\beta A}{\kappa_{a\nu}}}$ with taper ratio λ for straight-tapered wings.

For the case of straight-tapered wings with arbitrary section lift-curve-slope distribution for which the chord distribution is specified by taper ratio, evaluation of equation (5) is given in figure 2 where $\frac{(\kappa_\nu/\kappa_{a\nu})H_\nu}{(\beta A/\kappa_{a\nu})}$ for each of the three span stations is shown as a function of taper ratio.

EVALUATION OF ANTISYMMETRIC ANGLE-OF-ATTACK DISTRIBUTION α_ν

The antisymmetric angle-of-attack distributions most commonly encountered are those resulting from rolling wings, aileron deflection, and sideslip of wings with dihedral. Evaluation of the angle-of-attack distributions for these various cases is outlined in the sections immediately following.

Rolling wings.—For the case of the rigid wing, the induced velocity normal to the wing surface is equal to the upwash velocity experienced by the rolling wing. Thus, at span station ν

$$\alpha_\nu = \frac{w_\nu}{V} = -\left(\frac{pb}{2V}\right)\eta_\nu \tag{6}$$

where $pb/2V$ is the tip helix angle. It should be noted that the relation given by equation (6) assumes the wing structure to be rigid in that the distribution of α_ν is completely defined by the linear distribution of helix angle. In the case of flexible wings, however, the expression for α_ν must be modified to account for the streamwise angle-of-attack change which may occur due to bending or torsional deflections. In this case,

$$\alpha_\nu = -\left(\frac{pb}{2V}\right)\eta_\nu + \Delta\alpha_\nu \tag{7}$$

where $\Delta\alpha_\nu$ represents the modifying influence of flexibility. Normally, $\Delta\alpha_\nu$ is not considered for straight wings since only the effect of torsion (which is usually small) is involved. On swept wings, however, the effect of bending can cause $\Delta\alpha_\nu$ to be quite large so that the α_ν distribution may be affected considerably. Due to the interaction existing between the aerodynamic and structural forces, $\Delta\alpha_\nu$ cannot be determined directly, but must be found through equations of equilibrium or by iteration. With the loading for the rigid wing provided, however, the iteration procedure becomes relatively easy to apply. The first approximation of α_ν is found from the loading of the rigid wing and further refinements of α_ν may be found utilizing the successive loadings for the flexible wing as determined.

Deflected ailerons.—Where the spanwise distribution of the angle α_ν is to be considered equivalent to antisymmetric aileron deflection, it must suffer a discontinuity at the spanwise end of the control surface. The loading when such a discontinuity is present can be duplicated by a proper distribution of antisymmetric twist. In appendix C, the antisymmetric twist distribution required by the present theory to give accurate span loading distribution due to ailerons is found with the aid of zero-aspect-ratio wing theory given by reference 4. To minimize the computation involved, it is convenient to consider both the case of outboard and inboard ailerons.

1. *Outboard ailerons.*—With $m=7$, three different aileron spans can be conveniently defined for the outboard ailerons. For the aileron spans η_a, measured from the wing tip inboard, the antisymmetric twist distribution required per unit deflection of full-wing-chord ailerons, α_ν/δ, is given by

Case	I	II	III
η_a	0.169	0.444	0.805
$\frac{\alpha_1}{\delta}$	1.003	0.971	0.903
$\frac{\alpha_2}{\delta}$	.017	.926	.991
$\frac{\alpha_3}{\delta}$	.006	.014	.978

(8)

Inboard ailerons.—With $m=7$, three different aileron spans can be conveniently defined for the inboard ailerons. For the aileron spans η_a measured from the wing midspan outboard, the antisymmetric twist distribution required per unit deflection of full-wing-chord ailerons, α_ν/δ, is given by

Case	IV	V	VI
η_a	0.556	0.831	1.000
$\frac{\alpha_1}{\delta}$	0.044	0.013	1.016
$\frac{\alpha_2}{\delta}$	−.017	.961	.979
$\frac{\alpha_3}{\delta}$	1.087	1.095	1.101

(9)

Sideslip of wings with dihedral.—For calculating the rolling moment caused by dihedral angle for the sideslipping wing, the effect of the skewness of the vortex field in altering the effects of the dihedral angle will be assumed to be small (as assumed in reference 3). The problem then simplifies to

finding the rolling moment due to antisymmetric angle of attack with the unskewed vortex field. The solution to this problem is the same as for the ailerons which has already been solved.

The antisymmetric distribution of angle of attack for the sideslipping wing with dihedral is given by

$$\alpha_r=\bar{\beta}\Gamma \tag{10}$$

where

α_r effective angle-of-attack distribution
$\bar{\beta}$ angle of sideslip measured positive in the counterclockwise direction from the plane of symmetry
Γ dihedral angle

The wing parameter Γ is not affected by compressibility. Equation (10) is approximate for small values of $\bar{\beta}$ and Γ.

For unit $\bar{\beta}\Gamma$ over the span of the ailerons considered,

$$\bar{\beta}\Gamma=\delta \tag{11}$$

can be substituted for δ in equations (8) and (9).

APPLICATION OF METHOD

For the cases of antisymmetric angle-of-attack distributions resulting from rolling, aileron deflection, or sideslip with dihedral, it is possible to present a set of simultaneous equations which are required for the solution of the load distribution for an arbitrary plan form. With the loading known, integration formulas can be given to determine aerodynamic coefficients.

The loading-distribution coefficient G_n determined from the solutions of the simultaneous equations, are functions of p_{rn} which has been shown in a preceding section to be a function of wing geometry, compressibility, and section lift-curve slope. The aerodynamic coefficients are integrations of the load distribution and, therefore, will also be a function of wing geometry, compressibility, and section lift-curve-slope parameters. Application of the method to the general solution for arbitrary chord distribution is outlined and solutions are presented for the case of straight taper.

GENERAL SOLUTION

Aerodynamic characteristics due to rolling.—The solutions for the aerodynamic effects due to the rolling wing will be found and loading, rolling moment, spanwise center of pressure, and induced drag will be obtained.

1. *Simultaneous loading equations.*—The p_{rn} values are obtained from figure 1 and table I[7] with values of H_r given by equations (3) or (5).

The simultaneous equations (2), for the rigid and flexible wing, respectively, become:

$$\left.\begin{aligned}-0.924&=p_{11}\bar{G}_1+p_{12}\bar{G}_2+p_{13}\bar{G}_3\\ -0.707&=p_{21}\bar{G}_1+p_{22}\bar{G}_2+p_{23}\bar{G}_3\\ -0.383&=p_{31}\bar{G}_1+p_{32}\bar{G}_2+p_{33}\bar{G}_3\end{aligned}\right\} \tag{12}$$

where

$$\bar{G}_n=\frac{G_n}{pb/2V}$$

and

$$\left.\begin{aligned}-0.924+\frac{\Delta\alpha_1}{pb/2V}&=p_{11}\bar{G}_1+p_{12}\bar{G}_2+p_{13}\bar{G}_3\\ -0.707+\frac{\Delta\alpha_2}{pb/2V}&=p_{21}\bar{G}_1+p_{22}\bar{G}_2+p_{23}\bar{G}_3\\ -0.383+\frac{\Delta\alpha_3}{pb/2V}&=p_{31}\bar{G}_1+p_{32}\bar{G}_2+p_{33}\bar{G}_3\end{aligned}\right\} \tag{13}$$

where $\bar{G}_n=\frac{G_n}{pb/2V}$ and $\Delta\alpha_r$ is the incremental angle of attack due to aeroelastic effects.

2. *Loading distribution.*—The loading-distribution coefficient is given by $G=c_lc/2b$. Other forms of the loading coefficient are given by the identities

$$G=\frac{1}{2A}\frac{c_lc}{c_{av}}=\frac{C_l}{2A}\frac{c_lc}{C_lc_{av}} \tag{14}$$

The loading is known to be zero at $\eta=0$ and 1 and is determined at three intermediate span stations. Values of loading at other span stations can be obtained from a loading function derived in appendix B or, with equations (B23) or (B24) of appendix B, the loading can be found at span positions $\eta=0.981$, 0.831, 0.556, and 0.195.

3. *Rolling moment.*—The damping-in-roll derivative for the solutions of equations (12) or (13) is derived in appendix B and given by

$$\frac{\beta C_{l_p}}{\kappa_{av}}=\frac{\pi}{16}\left(\frac{\beta A}{\kappa_{av}}\right)[\bar{G}_2+0.707(\bar{G}_1+\bar{G}_3)] \tag{15}$$

4. *Spanwise center of pressure.*—The equation giving center of pressure on the wing semispan is shown in appendix B to be

$$\eta_{c.p.}=\frac{\beta C_l/\kappa_{av}}{\frac{\beta A}{\kappa_{av}}(0.163\bar{G}_1+0.248\bar{G}_2+0.430\bar{G}_3)}$$

$$=\frac{1}{0.082\left(\frac{c_lc}{C_lc_{av}}\right)_1+0.124\left(\frac{c_lc}{C_lc_{av}}\right)_2+0.215\left(\frac{c_lc}{C_lc_{av}}\right)_3} \tag{16}$$

5. *Induced drag.*—The induced drag is derived in appendix B and given by

$$\frac{\beta C_{D_i}}{\kappa_{av}}=\frac{\pi}{2}\left(\frac{\beta A}{\kappa_{av}}\right)\left[G_1^2+G_2^2+G_3^2-\frac{\sqrt{2}}{2}G_2(G_1+G_3)\right] \tag{17}$$

Aerodynamic characteristics due to aileron deflection.—The solutions for the aerodynamic effects due to ailerons will be found for three different spans of outboard and inboard ailerons. Cross plots of these data provide curves for arbitrary aileron spans.

1. *Simultaneous loading equations.*—The p_{rn} values are obtained from figure 1 and table I with values of H_r given by equations (3) or (5).

(*a*) *Deflected outboard ailerons.*—The aileron spans measured from the wing tip inboard are given by η_a. The simultaneous solution for antisymmetric spanwise loading due to

[7] Values of p_{rn} beyond the scope of figure 1 are included in table I. For values of H_r larger than those included in figure 1 and table I, the p_{rn} curves can be obtained from equation (B8) which gives the linear asymptotes of the p_{rn} function.

deflection of any of the three following aileron spans can be obtained from the appropriate set of the following equations:

Case	I	II	III	
η_a	0.169	0.444	0.805	
$\frac{\alpha_1}{\delta}$	1.003	0.971	0.998	$=p_{11}\overline{G}_1+p_{12}\overline{G}_2+p_{13}\overline{G}_3$
$\frac{\alpha_2}{\delta}$	.017	.996	.991	$=p_{21}\overline{G}_1+p_{22}\overline{G}_2+p_{23}\overline{G}_3$ (18)
$\frac{\alpha_3}{\delta}$	.006	.014	.978	$=p_{31}\overline{G}_1+p_{32}\overline{G}_2+p_{33}\overline{G}_3$

where $\overline{G}_n=G_n/\delta$.

(*b*) *Deflected inboard ailerons.*—The aileron spans measured from the wing midspan outboard are given by η_a. The simultaneous solution for antisymmetric spanwise loading due to deflection of any of the three following aileron spans can be obtained from the appropriate set of the following equations:

Case	IV	V	VI	
η_a	0.556	0.831	1.000	
$\frac{\alpha_1}{\delta}$	0.044	0.013	1.016	$=p_{11}\overline{G}_1+p_{12}\overline{G}_2+p_{13}\overline{G}_3$
$\frac{\alpha_2}{\delta}$	−.017	.961	.979	$=p_{21}\overline{G}_1+p_{22}\overline{G}_2+p_{23}\overline{G}_3$ (19)
$\frac{\alpha_3}{\delta}$	1.087	1.095	1.101	$=p_{31}\overline{G}_1+p_{32}\overline{G}_2+p_{33}\overline{G}_3$

where $\overline{G}_n=G_n/\delta$.

2. *Loading distribution.*—The spanwise loading distributions due to various aileron configurations include:

(*a*) *Full-wing-chord ailerons.*—The loading is known to be zero at $\eta=0$ and 1, and is determined at three intermediate span stations. With equation (C13) and tables C6, B1, and C7, the loading can be found at span stations $\eta=0.981$, 0.831, 0.556, and 0.195 for each of the aileron spans considered. With these given points and the knowledge that the slope of the loading distribution curve is theoretically infinite at the point of angle-of-attack discontinuity (aileron spanwise end), the loading distribution can be faired.

(*b*) *Constant fraction of wing-chord ailerons.*—The spanwise loading of constant fraction of wing-chord ailerons is equal to the product of the loading due to full-wing-chord ailerons and the effective change of angle of attack with aileron angle,[8] $d\alpha/d\delta$. The factor $d\alpha/d\delta$ is a function of the ratio of aileron chord to wing chord $t=c_a/c$. The change of section angle of attack with aileron angle $d\alpha/d\delta$ is presented in figure 3, which is reproduced from figure 18 of reference 5.

Although figure 3 taken from reference 5 limits the Mach number range to Mach numbers less than 0.2, this limitation is believed to be unwarranted since theory indicates that $d\alpha/d\delta$ is unaffected by compressibility for the two-dimensional wing. However, as indicated in reference 4, $d\alpha/d\delta$ is strongly affected by low aspect ratio and will change appreciably if the parameter βA becomes much less than two; hence, the values of $d\alpha/d\delta$ from figure 3 appear to be valid for $\beta A>2$.

[8] In using $d\alpha/d\delta$ here, it should be noted that the assumption is made that the effective airfoil section is taken as being parallel to the plane of symmetry and that the section approaches a two-dimensional section. The validity of this assumption can be questioned; however, limited checks with experiment show it to be at least approximately correct.

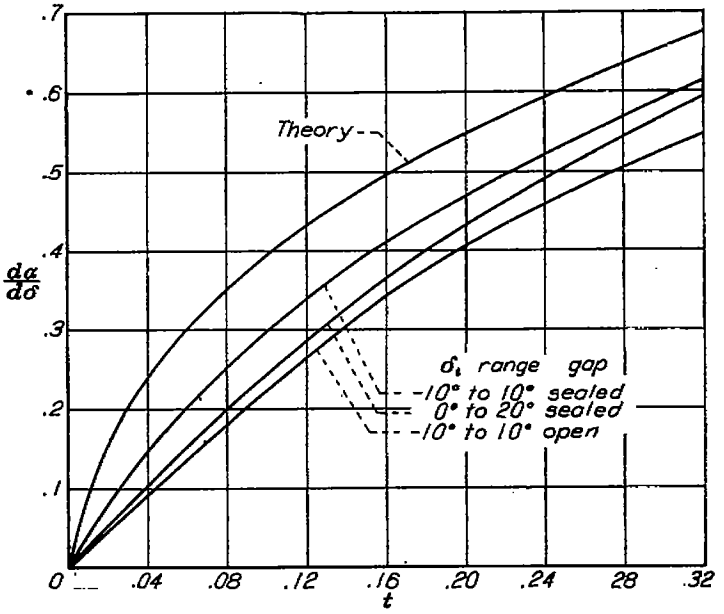

FIGURE 3.—Variation of lift-effectiveness parameter with aileron chord ratio, $t=\frac{c_a}{c}$. Average trailing-edge angle about 10°; $M\leq 0.2$. Curves from reference 5.

(*c*) *Arbitrary spanwise distribution of aileron chord.*—The aileron can be divided into several spans with constant $d\alpha/d\delta$, then the total loading is the sum of the products of the full-wing-chord loading of each span and its respective $d\alpha/d\delta$.

3. *Rolling moment.*—The rolling moment can be found for the following aileron configurations:

(*a*) *Full-wing-chord ailerons.*—The spanwise loading due to aileron deflection cannot be integrated with sufficient accuracy with equation (15). In appendix C, a similar integration formula is developed that applies to each given aileron span. Equation (C10) and table C5 give

$$\frac{\beta C_{l_\delta}}{\kappa_{av}}=\left(\frac{\beta A}{\kappa_{av}}\right)(h_1\overline{G}_1+h_2\overline{G}_2+h_3\overline{G}_3) \tag{20}$$

where for each of the cases of equations (18) and (19) the h_n values are given by

Case	I	II	III	IV	V	VI
h_1	0.140	0.139	0.138	0.146	0.141	0.140
h_2	.199	.196	.196	.200	.197	.196
h_3	.145	.139	.138	.140	.139	.140

(*b*) *Constant fraction of wing-chord ailerons.*—For constant fraction of wing-chord ailerons with aileron angle measured parallel to the plane of symmetry, the aileron effectiveness is given by

$$\frac{\beta C_{l_{\delta_i}}}{\kappa_{av}}=\frac{d\alpha}{d\delta}\left(\frac{\beta C_{l_\delta}}{\kappa_{av}}\right) \tag{21}$$

(*c*) *Arbitrary spanwise distribution of aileron chord.*—The deflection of ailerons for which t varies spanwise on the wing can be considered as an equivalent wing-twist distribution. The effective antisymmetric twist of the wing is given by

$$\alpha_r=\frac{d\alpha}{d\delta}\delta_i \tag{22}$$

where $d\alpha/d\delta$ is now a function of spanwise position. The antisymmetric angle-of-attack distribution given by equation (22) can be divided into spanwise steps of constant angle of attack and the total rolling moment can be found by the summation of the rolling moment due to each spanwise step. The rolling moments of the spanwise steps are obtained from a curve of rolling-moment coefficient $\beta C_{l_\delta}/\kappa_{as}$ as a function of unit antisymmetric angle of attack from the wing root outboard. This step method is the procedure used in reference 1.

A curve of $\beta C_{l_\delta}/\kappa_{as}$ as a function of unit antisymmetric angle of attack from the wing root outboard can be obtained from the solutions of equation (19) for the cases IV, V, and VI. An additional point can be obtained from the solution of case III of equation (18), applying the relations (discussed later) existing between inboard and outboard ailerons. The rolling moment due to the twist given by equation (22) can be obtained, by a method other than the step method, from the integral given by

$$\frac{\beta C_{l_{\delta_t}}}{\kappa_{as}} = \int_0^1 \frac{d\alpha}{d\delta} \frac{d(\beta C_{l_\delta}/\kappa_{as})}{d\eta}\, d\eta \tag{23}$$

which can be integrated numerically by taking the graphical slopes of $\beta C_{l_\delta}/\kappa_{as}$ which is a function of extent of unit antisymmetric angle of attack from the wing root outboard.

4. *Spanwise center of pressure and induced drag.*—Spanwise center of pressure and induced-drag integration formulas for loading due to ailerons are not given; however, equations (16) and (17) can give approximate integrations of the loading to obtain center of pressure and induced drag.

5. *Additional considerations:*

(*a*) *Relation between aerodynamic characteristics for outboard and inboard ailerons.*—The spanwise loading distributions due to outboard and inboard ailerons bear a simple relation to each other. Since loading is linearly proportional to angle of attack, loadings are directly additive. Then, for outboard and inboard ailerons with the spanwise ends of the ailerons at the same span station,

$$\left.\begin{aligned} G_{\text{inboard}} &= G_{(\eta_a=1)} - G_{\text{outboard}} \\ C_{l_{\delta_{\text{inboard}}}} &= C_{l_{\delta_{(\eta_a=1)}}} - C_{l_{\delta_{\text{outboard}}}} \\ \eta_{a_{\text{inboard}}} &= 1 - \eta_{a_{\text{outboard}}} \end{aligned}\right\} \tag{24}$$

These relations do not apply for $\eta_{c.p.}$ and C_{D_i} since these characteristics are not linearly proportional to loading.

(*b*) *Differential aileron angles.*—The effect of a differential between aileron angles can be taken into account by considering the C_{l_δ} of each wing panel as one-half the antisymmetric results of equations (20), (21), or (23). The total wing rolling moment is then the sum of the products of $C_{l_\delta}/2$ given by equations (20), (21), or (23) and the angle of deflection of each aileron. Although the total rolling moment can be found by this procedure, the spanwise loading distribution can be found only approximately by the products of the antisymmetric unit loading G/δ and the deflection of each aileron. However, the loading distribution so found will be quite accurate since this procedure neglects only the small change due to the induced effects of the differentially different opposite wing panels.

(*c*) *Aileron angles measured perpendicular to the hinge line.*—The relationship between aileron angle measured perpendicular to the aileron hinge line and that measured parallel to the plane of symmetry is given by

$$\tan \underline{\delta} = \frac{\tan \delta}{\cos \Lambda_t} \tag{25}$$

where

Λ_t sweep angle of the aileron hinge line

$\underline{\delta}$ angle measured perpendicular to the hinge line

For constant fraction of wing-chord ailerons on straight-tapered wings, Λ_t is given by

$$\tan \Lambda_t = \tan \Lambda_{c/4} - \frac{4(0.75-t)}{A}\left(\frac{1-\lambda}{1+\lambda}\right) \tag{26}$$

where t is the fraction of wing-chord aileron measured from the wing trailing edge.

Aerodynamic characteristics due to sideslip of wings with dihedral.—The total antisymmetric loading due to sideslip can be considered as the sum of that due to dihedral angle and that due to zero dihedral angle. For the unswept wing, the rolling moment due to sideslip for zero dihedral angle is generally considered negligible; however, for the swept wing, this effect can be appreciable. In the present report, only that part due to dihedral angle will be considered for the swept and nonswept wings.

1. *Simultaneous loading equations.*—The p_{rn} values are obtained from figure 1 and table I with values of H_r given by equations (3) or (5).

The simultaneous equations resulting from the substitution of $\delta = \bar{\beta}\Gamma$ (see equation (11)) and $\overline{\overline{G}} = G/\bar{\beta}\Gamma$ in equations (18) and (19) are applicable in the determination of the effects of unit outboard or inboard dihedral angle over the span of the ailerons considered.

2. *Rolling moment.*—The rolling moment due to various dihedral angle distributions include:

(*a*) *Constant spanwise dihedral angle.*—For dihedral angle constant for the entire wing semispan, the loading is given by the solution of case VI in equation (19) for $\overline{\overline{G}} = G/\bar{\beta}\Gamma$ and the rolling moment from equation (20) becomes

$$\frac{\beta C_{l_{\bar{\beta}}}}{\kappa_{as}\Gamma} = \frac{\beta A}{\kappa_{as}}(0.140\overline{\overline{G}}_1 + 0.198\overline{\overline{G}}_2 + 0.140\overline{\overline{G}}_3) \tag{27}$$

(*b*) *Gulled wing.*—For the gulled wing, solutions of equation (19) for $\overline{\overline{G}} = G/\bar{\beta}\Gamma$ gives the loading, and the rolling moment from equation (20) becomes

$$\frac{\beta C_{l_{\bar{\beta}}}}{\kappa_{as}\Gamma} = \frac{\beta A}{\kappa_{as}}(h_1\overline{\overline{G}}_1 + h_2\overline{\overline{G}}_2 + h_3\overline{\overline{G}}_3) \tag{28}$$

A plot of the results of cases IV, V, and VI gives the extent of unit dihedral angle from the wing root outboard. Then, for a gulled wing, the total rolling moment equals the sum of products of dihedral angle of each span section and the rolling-moment contribution of the respective span sections.

(*c*) *Variable spanwise dihedral angle.*—If Γ varies span-

wise, the rolling moment can be obtained by integration as in equation (23). The integral becomes

$$\frac{\beta C_{l_{\bar{\beta}}}}{\kappa_{av}} = \int_0^1 \Gamma(\eta) \frac{d(\beta C_{l_{\bar{\beta}}}/\kappa_{a_s}\Gamma)}{d\eta} d\eta \qquad (29)$$

where $\frac{d(\beta C_{l_{\bar{\beta}}}/\kappa_{a_s}\Gamma)}{d\eta}$ is the slope of the curve described in part (*b*) above.

SOLUTION FOR STRAIGHT-TAPERED WINGS

Charts of aerodynamic characteristics for straight-tapered wings can be presented in terms of geometric, compressibility, and average section lift-curve-slope parameters. These charts provide a ready means of obtaining data directly.

Aerodynamic characteristics due to rolling.—The application of equation (12) for a constant value of section lift-curve slope[9] provides the spanwise loadings at span stations 0.383, 0.707, and 0.924 which are presented in figure 4 for a wide range of plan forms. The interpolation formula of equation (B24) will give values of loading due to rolling at span stations other than those presented. With equation (15), the damping-in-roll coefficients $\beta C_{l_p}/\kappa_{av}$ can be obtained and are presented in figure 5 for a wide range of plan forms.

Aerodynamic characteristics due to aileron deflection.—The application of equation (19), case III of equation (18), and equation (20) provide aileron effectiveness in the coefficient form $\beta C_{l_\delta}/\kappa_{av}$ for several aileron spans. In figure 6, $\beta C_{l_\delta}/\kappa_{av}$ is plotted against extent of unit antisymmetric angle of attack from the wing semispan root outboard for a range of wing parameters.

As presented, figure 6 gives directly the effectiveness of full-wing-chord inboard ailerons for aileron spans measured from the plane of symmetry outboard. The effectiveness of full-wing-chord outboard ailerons for aileron spans measured from the wing tip inboard is given by figure 6 directly by the relations of equation (24). For full-wing-chord ailerons located arbitrarily on the wing semispan, the aileron effectiveness can be obtained directly from figure 6 as indicated in the following example sketch.

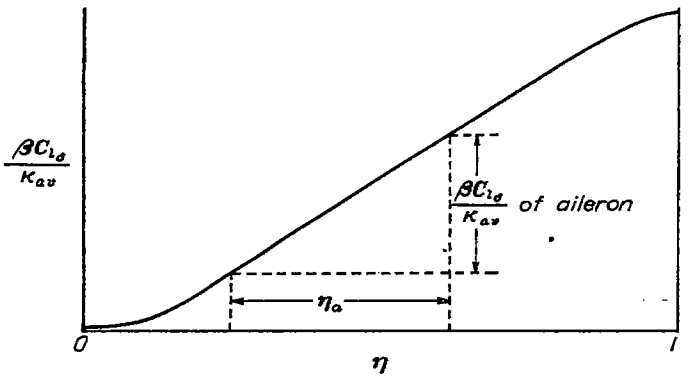

With the full-wing-chord values given above, the effectiveness of constant fraction of wing-chord ailerons or ailerons of arbitrary spanwise chord distribution can be found through use of equations (21) or (23) with the $d\alpha/d\delta$ values of figure 3.

[9] Throughout the figures, κ_{a_s} is the constant spanwise section lift curve slope or the average of a small variation. For large spanwise variations of κ that follow the function given by equation (B11) developed in appendix B, the parameters $\beta A/\kappa_{a_s}$ and λ can be replaced by the parameters $\frac{\beta A}{(\kappa_R+\kappa_T\lambda)/(1+\lambda)}$ and $\frac{\kappa_T}{\kappa_R}\lambda$, respectively. For large spanwise variations of κ that do not follow the curve of equation (B11), the simultaneous equations for the general solution can be solved for arbitrary distributions of κ. The H_r values can be obtained from figure 2.

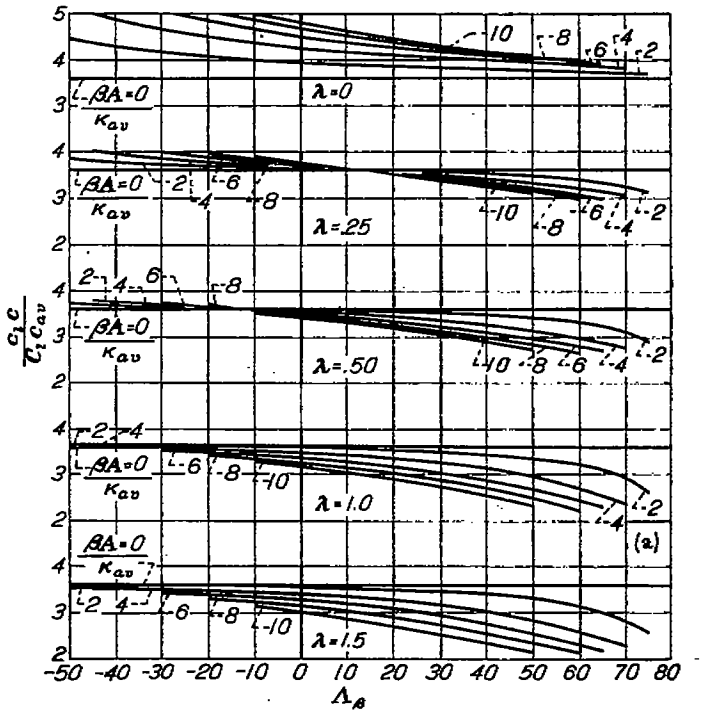

(a) η=0.3827.

FIGURE 4.—Variation of loading due to rolling coefficient $\frac{c_l c}{C_l c_{av}}$ with compressible sweep parameter Λ_β, degrees, for straight-tapered wings.

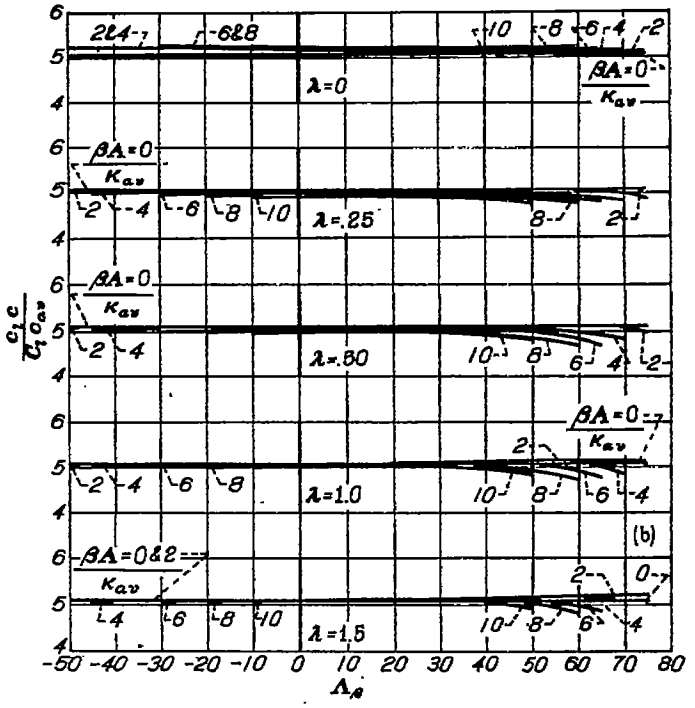

(b) η=0.7071.

FIGURE 4.—Continued.

Aerodynamic characteristics due to sideslip of wings with dihedral.—The application of equation (19), case III of equation (18), but with $\delta=\bar{\beta}\Gamma$, and $\bar{\bar{G}}=G/\bar{\beta}\Gamma$, and the use of equation (28) provides rolling moments due to dihedral angle for the wing in sideslip. These rolling moments are given in the coefficient form $\beta C_{l_{\bar{\beta}}}/\kappa_{a_s}\Gamma$ which is the same function of η as $\beta C_{l_\delta}/\kappa_{a_s}$ and is presented with $\beta C_{l_\delta}/\kappa_{a_s}$ in figure 6. Figure 6 with equation (29) will provide the rolling moment

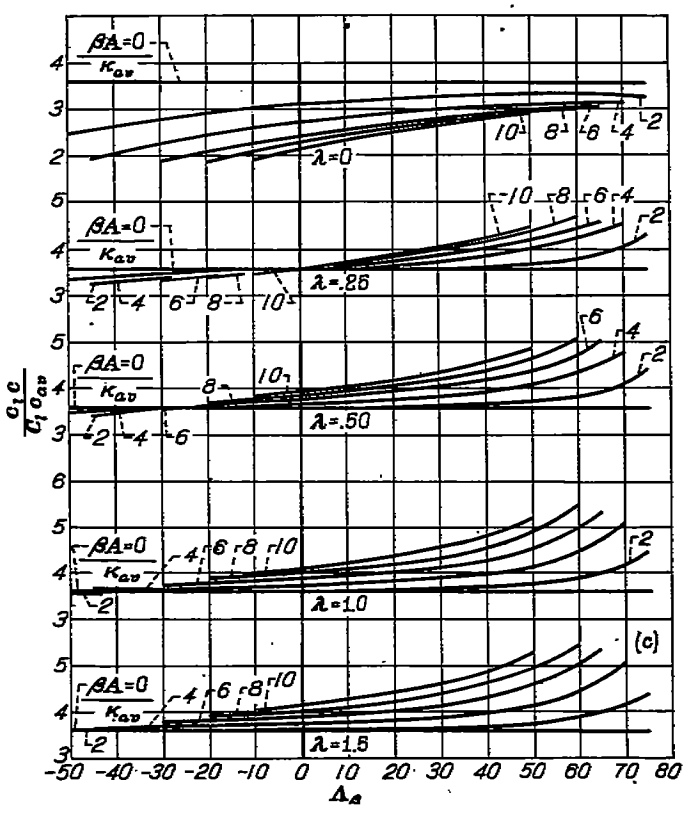

(c) $\eta=0.9239$.

FIGURE 4.—Concluded.

due sideslip for any symmetric spanwise distribution of dihedral angle.

For dihedral angle constant spanwise, the rolling moment is given by the value at $\eta=1$ in figure 6. These values for constant spanwise dihedral angle are presented in figure 7 as a function of aspect ratio for various values of sweep angle and taper ratio.

DISCUSSION

Effects of plan-form parameters on aerodynamic characteristics for straight-tapered wings are shown by plots against the various parameters. Compressibility is discussed and formulas given for a range of plan forms at sonic speeds. Theoretical considerations and experimental comparisons indicate the order of reliability of the present theoretical results.

STRAIGHT-TAPERED WINGS

The spanwise loading distribution due to rolling for several plan forms is presented in figure 8. These curves are the result of applying figure 4 and the loading interpolation formula of appendix B. The loading coefficient is given as $\frac{\eta_{c.p.}}{(\eta_{c.p.})_{A=0}}\left(\frac{c_l c}{C_l c_{av}}\right)$ to make the total loading on the semispan constant and thus show more clearly the changes of distribution due to sweep and taper ratio. Figure 8 shows large changes in loading distribution for the zero tapered wing. The effects of sweep are generally as expected, namely, that sweepback shifts the loading outboard.

Effects of plan form on the rolling moment due to rolling is shown from cross plots of figure 5 which are presented in figures 9 and 10. For higher aspect ratio, figures 4, 9, and 10 show the marked lowering of rolling moment due to sweep. Figure

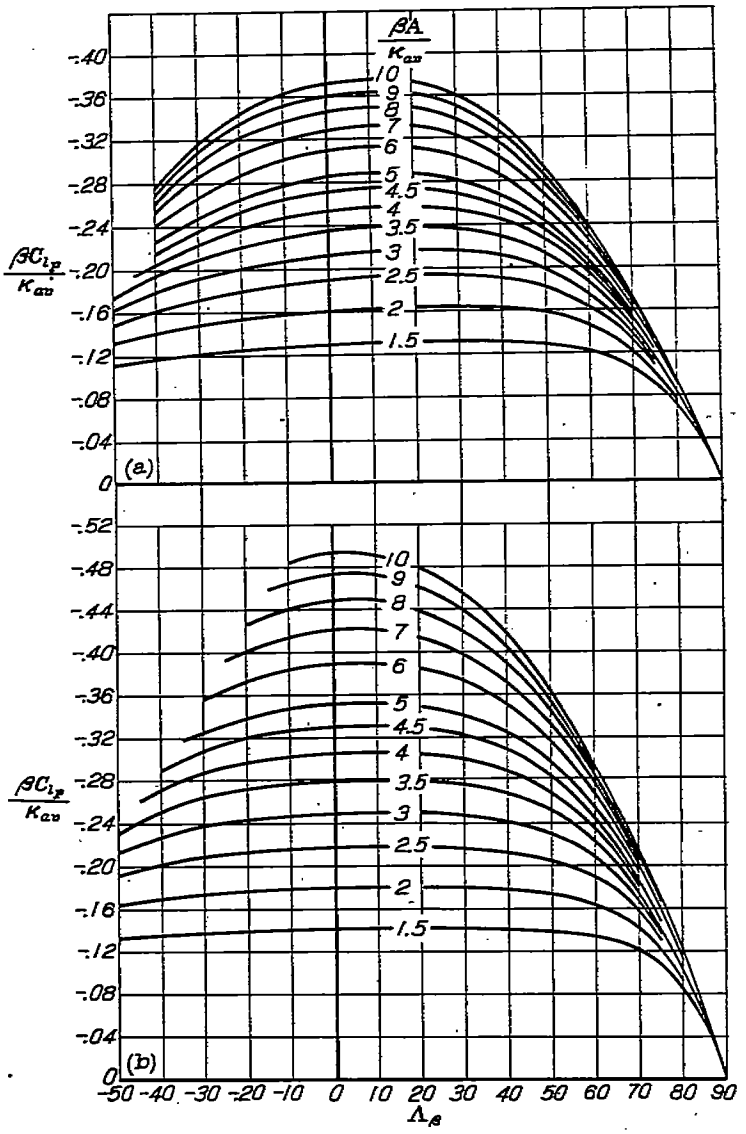

(a) $\lambda=0$.

(b) $\lambda=0.25$.

FIGURE 5.—Variation of damping-in-roll parameter $\frac{\beta C_{l_p}}{\kappa_{av}}$ with compressible sweep parameter A_β, degrees, for straight-tapered wings.

9 indicates that for low aspect ratio, the rolling moment becomes essentially independent of sweep and taper. The taper effects on rolling moment as seen in figure 10 are small except for values of taper ratio less than 0.25.

Typical spanwise loading distributions due to full-wing-chord aileron deflection are shown in figure 11. These curves were faired with the aid of the loading interpolation function of appendix C and, at the aileron spanwise end, care was taken to make the slope large.

Wing geometry effects on aileron effectiveness for full-chord outboard partial-span ailerons (with aileron angle measured parallel to the plane of symmetry) are given in figure 12. The geometry effects on $\beta C_{l_\delta}/\kappa_{av}$ are similar to those on the damping-in-roll coefficient. Comparison of figure 12 (a) with figure 9 shows that C_{l_δ} approaches the zero-aspect-ratio value in the same manner as does C_{l_p}. Figure 13 gives comparative effectiveness of inboard and outboard ailerons for swept wings. As sweep increases, the difference of effectiveness between inboard and out-

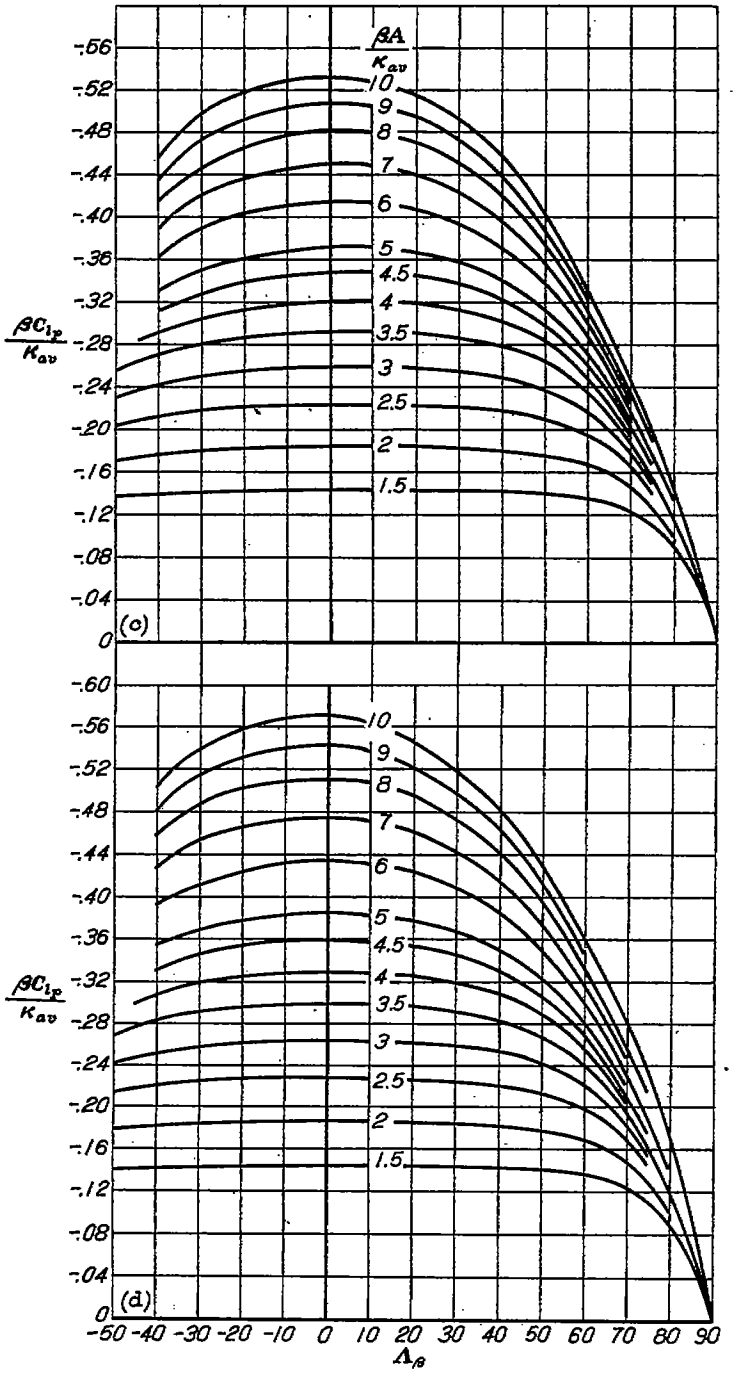

(c) λ=0.50.

(d) λ=1.0.

FIGURE 5.—Continued.

board ailerons decreases showing that inboard ailerons for highly swept-back wings approach the effectiveness of outboard ailerons. Since $d\alpha/d\delta$ becomes large rapidly at small values of t (fig.3), then, for a given aileron area, narrow full-span ailerons for swept-back wings may be more desirable than larger-chord outboard ailerons. The relative effects of figures 12 and 13 apply equally well for constant fraction of chord ailerons, since the data would differ only by a constant factor $d\alpha/d\delta$.

COMPRESSIBILITY

From the three-dimensional linearized-compressible-flow equation, it can be shown that the effects of compressibility will be properly taken into account if the longitudinal com-

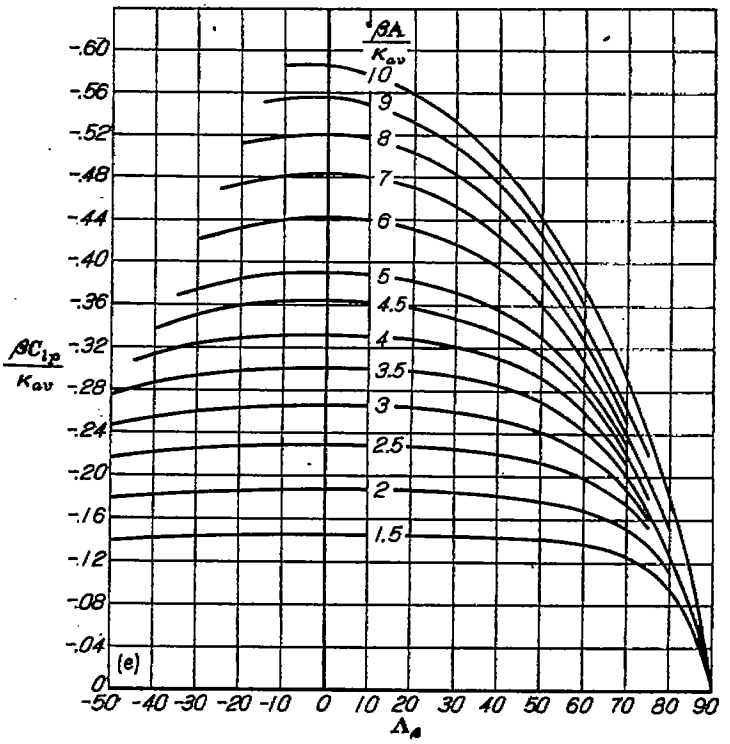

(e) λ=1.5.

FIGURE 5.—Concluded.

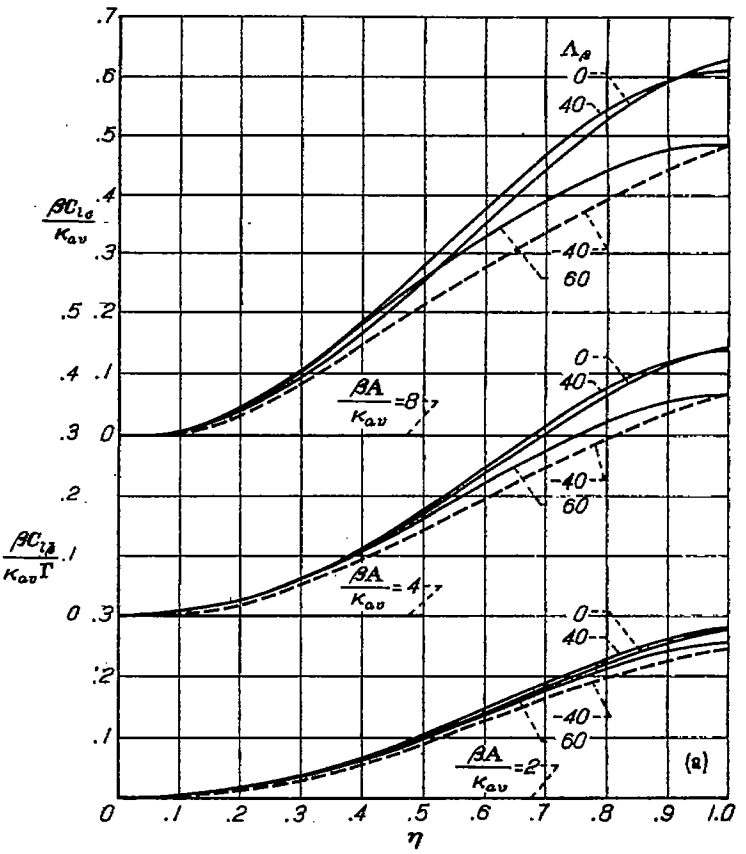

(a) λ=0.

FIGURE 6.—Aileron rolling-moment parameter $\frac{\beta C_{l_\delta}}{\kappa_{av}}$, per radian, and rolling moment due to sideslip with dihedral $\frac{\beta C_{l_{\bar{\beta}}}}{\kappa_{av}\Gamma}$, per radian squared, for extent of unit antisymmetric angle of attack from the wing root outboard.

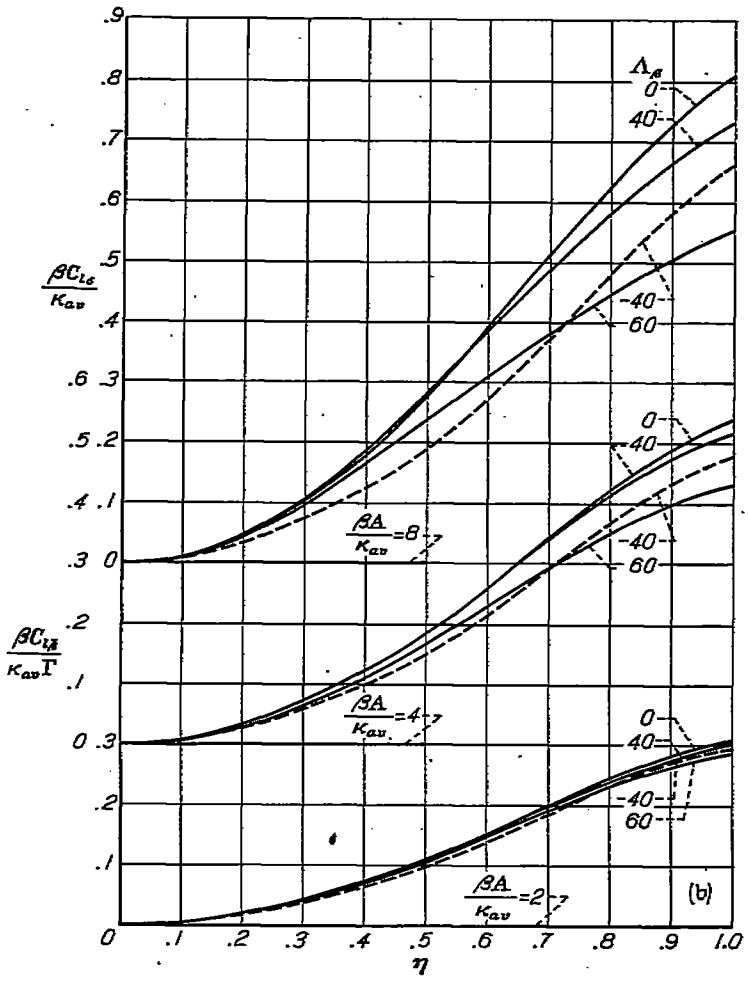

(b) $\lambda=0.5$.

FIGURE 6.—Continued.

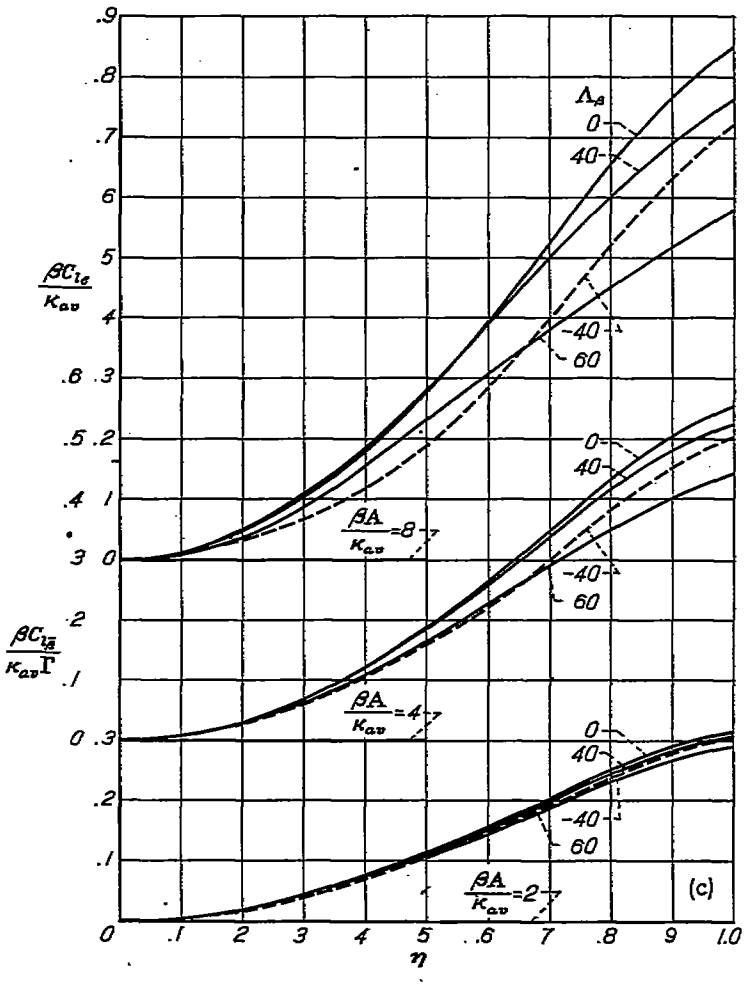

(c) $\lambda=1.0$.

FIGURE 6.—Concluded.

ponents of a wing plan form are increased by the factor $1/\beta$. Or, alternatively, if the linearized compressible flow equation be divided through by β^2, then the lateral and vertical components of a plan form are decreased by the factor β. In both cases, the incompressible local lift is increased by the factor $1/\beta$ and the compressible local lift coefficient can be written as the parameter βc_l.

With these relations known, an incompressible theory can be made into a compressible theory subject to the limitations of the linearized compressible flow equation. The geometric parameters of a wing are simply substituted by $\beta A, \Lambda_\beta = \tan^{-1}\frac{\tan\Lambda}{\beta}$ and βb. With local lift coefficient given by βc_l, the dimensionless loading becomes $G=\frac{\beta c_l c}{2\beta b}=\frac{c_l c}{2b}$. The wing-chord distribution remains unaltered.

The sonic speed results of reference 4 can be used as a limit point in the present theory for a curve of the variation of antisymmetric aerodynamic characteristics with Mach number. The following equations apply at the speed of sound to plan forms with all points of the trailing edge at or behind the upstream line of maximum wing span:

$$C_{l_\beta}=\frac{-\pi A}{32}$$

For outboard ailerons,

$$C_{l_\beta}=\frac{A}{6}\sin^3\theta, \text{ where } \eta_a=1-\cos\theta$$

For inboard ailerons,

$$C_{l_\beta}=\frac{A}{6}(1-\sin^3\theta), \text{ where } \eta_a=\cos\theta$$

Reference 4 shows that aileron effectiveness at the speed of sound is independent of the chordwise location of the aileron hinge line, provided the hinge line remains ahead of all points of the trailing edge.

ACCURACY OF THE SEVEN-POINT SOLUTION FOR AILERONS

The prediction of aileron effectiveness for given aileron spans with wing twist determined by zero-aspect-ratio theory at only seven span points to satisfy the boundary conditions has been theoretically shown to be sufficient by comparing results with the computation of a typical 3.5 aspect ratio, 45° swept wing with 15 span points satisfying the boundary conditions. The process of finding aileron spans for the 15-point method was the same as that in appendix C. The curves showing the variation of C_{l_β} with aileron span for the 7- and 15-point computations were identical.

The solution for the angle-of-attack distribution that includes a discontinuity can be compared with the solution

for the continuous angle-of-attack distribution by considering an aileron such that the angle-of-attack distribution is equivalent to that of the rolling wing. The damping-in-roll coefficient then can be found by use of equation (23) which reduces to the form

$$C_l = \int_0^1 \alpha \frac{dC_{l_\delta}}{d\eta}\, d\eta$$

for $\alpha = -\left(\frac{pb}{2V}\right)_\eta$, and integrating by parts

$$C_{l_p} = \int_0^1 C_{l_\delta} d\eta - C_{l_{\delta_{\eta=1}}}$$

This relation states that C_{l_p} is equal to the area between a curve of figure 6 and the line of C_{l_δ} for $\eta = 1$. The curves of figure 6 were found by the simplified lifting-surface theory with antisymmetric twist determined by zero-aspect-ratio theory. The values of C_{l_p} obtained in this manner from figure 6 were identical to the C_{l_p} values given by simplified lifting-surface theory for continuous linear antisymmetric-twist distribution.

As further theoretical check, the values of rolling moment due to constant spanwise dihedral angle are obtained from 15-point computations in reference 3 for taper ratio equal to one, with which the present theory for the 7-point method is in exact agreement.

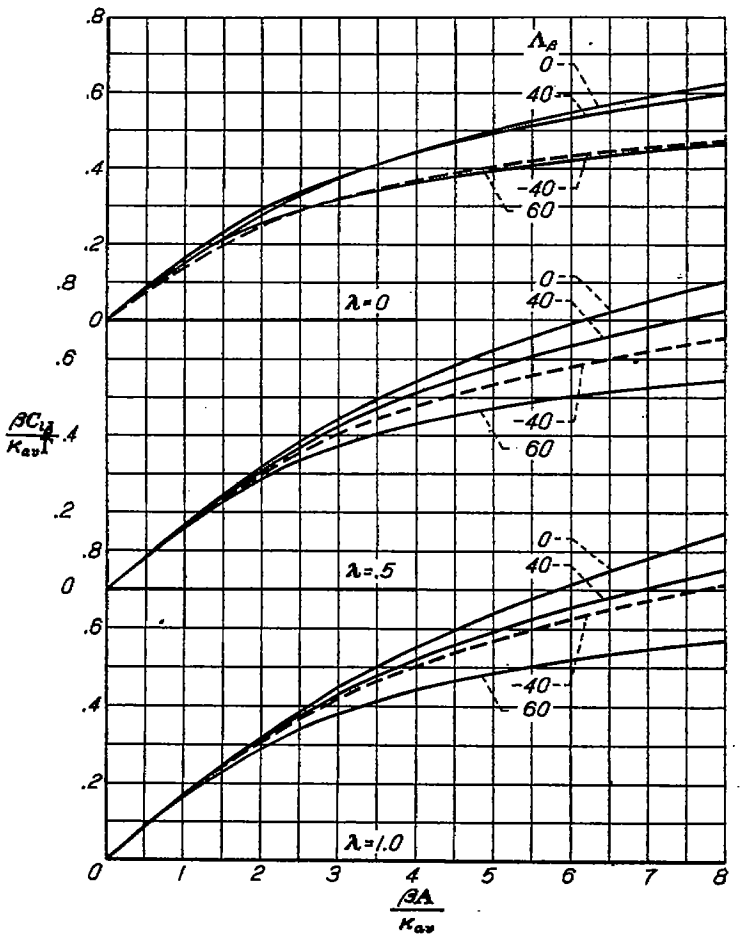

FIGURE 7.—Rolling moment due to sideslip of wing with dihedral $\frac{\beta C_{l_\delta}}{K_{ay}}$, per radian squared, for unit constant spanwise dihedral angle for straight-tapered wings.

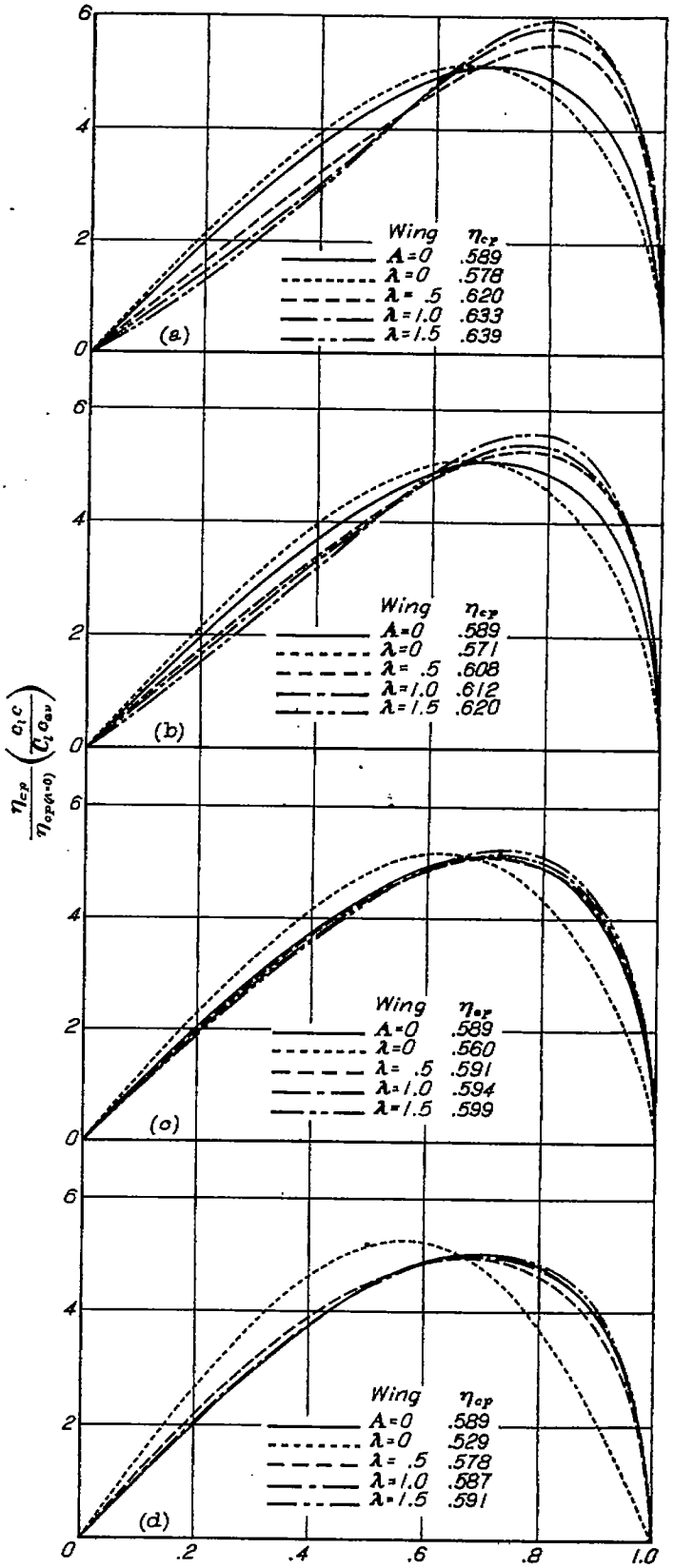

(a) $\Lambda_\beta = 60°$.
(b) $\Lambda_\beta = 45°$.
(c) $\Lambda_\beta = 0°$.
(d) $\Lambda_\beta = -45°$.

FIGURE 8.—Spanwise loading due to rolling of wings with various taper-ratio and sweep-angle parameters of aspect-ratio parameter $\frac{\beta A}{K_{ay}} = 4$. The curve for $A = 0$ serves as a basis for comparison and the factor $\frac{\eta_{cp}}{\eta_{cp(A=0)}}$ gives the curves constant area equal to 3.454.

COMPARISON OF THEORETICAL AND EXPERIMENTAL RESULTS

The electro-magnetic analogy method of reference 6 provides damping-in-roll coefficients for an aspect-ratio range of unswept, tapered wings. The results of the present theory and those of reference 8 are compared in figure 14. Except for the taper ratio effects on C_{l_p} the comparison is good. The rounded-wing-tip values of C_{l_p} given by NACA Rep. 635 (reference 1) are included in figure 14. Since rounded wing tips generally give values of C_{l_p} about 6 percent lower than straight wing tips, the values of NACA Rep. 635 appear to be appreciably too high for lower-aspect-ratio wings. The present theory and the theory of reference 6 approach the value given by the zero-aspect-ratio theory of reference 4 quite satisfactorily. The results of the present theory may be further assessed by the comparison with the results of low-speed experiment as given in figure 15 for the range of plan forms presented. For further experimental verification of the accuracy with which C_{l_p} can be determined by the present theory, the reader is referred to reference 3 which supports the theory as well or better than figure 15 of the present report.

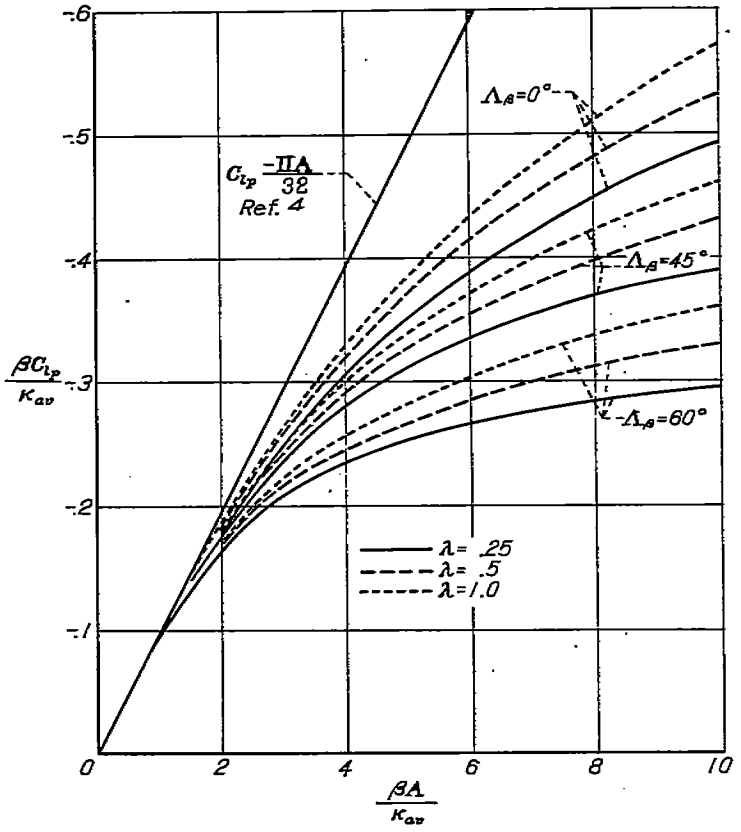

FIGURE 9.—Variation of the damping-in-roll parameter $\frac{\beta C_{l_p}}{K_{av}}$ with aspect-ratio parameter $\frac{\beta A}{K_{av}}$ for various sweep angles and taper ratios.

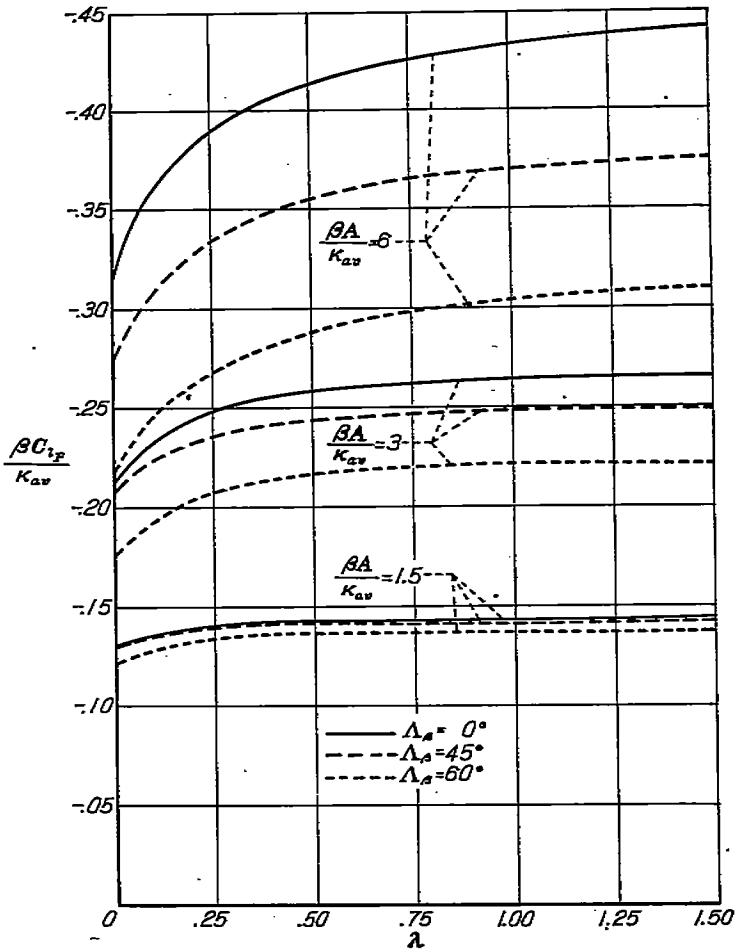

FIGURE 10.—Variation of the damping-in-roll parameter $\frac{\beta C_{l_p}}{K_{av}}$ with taper ratio for wings with various aspect-ratio and sweep-angle parameters.

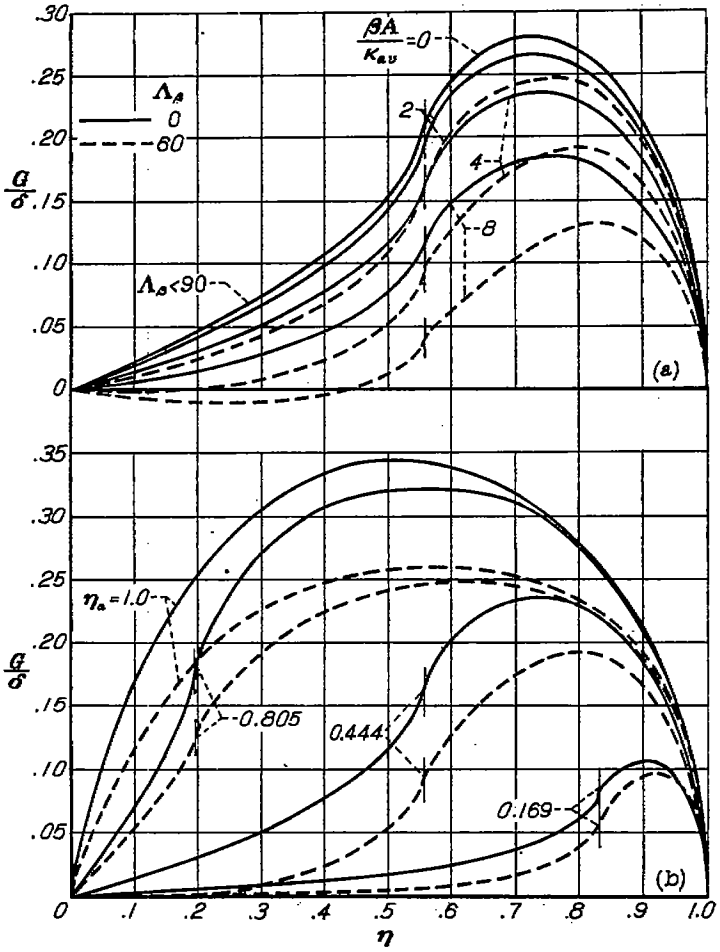

FIGURE 11.—Antisymmetric spanwise loading distribution due to deflection of outboard ailerons, for $c_a=c$, on wings having a taper ratio of 0.5. (a) $\eta_a=0.444$. (b) $\frac{\beta A}{\kappa_{av}}=4.0$.

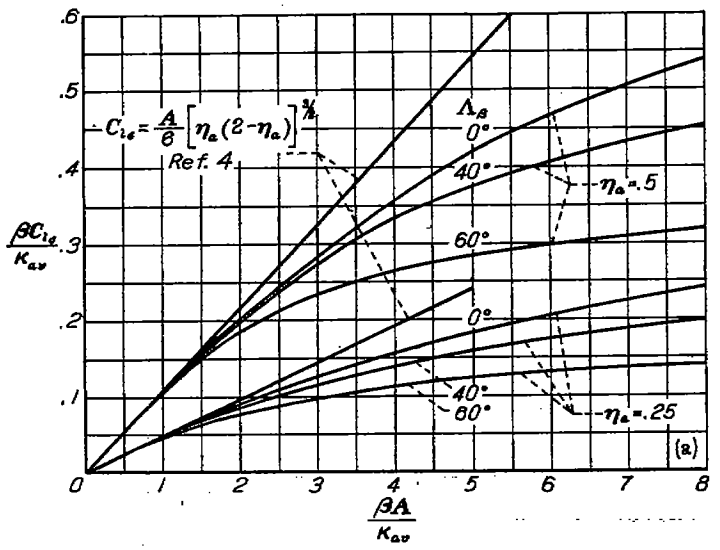

FIGURE 12.—Aileron rolling-moment-coefficient parameter $\frac{\beta C_{l_\xi}}{\kappa_{av}}$, per radian, for outboard ailerons as a function of aspect-ratio parameter, taper ratio, and compressible-sweep parameter. (a) $\lambda=0.5$.

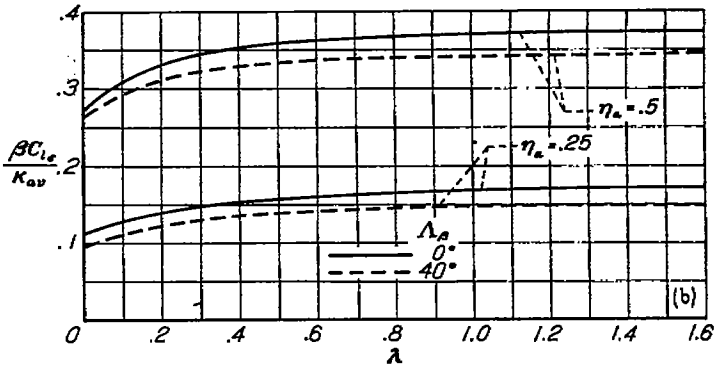

(b) $\frac{\beta A}{\kappa_{av}}=4.0$.

FIGURE 12.—Continued.

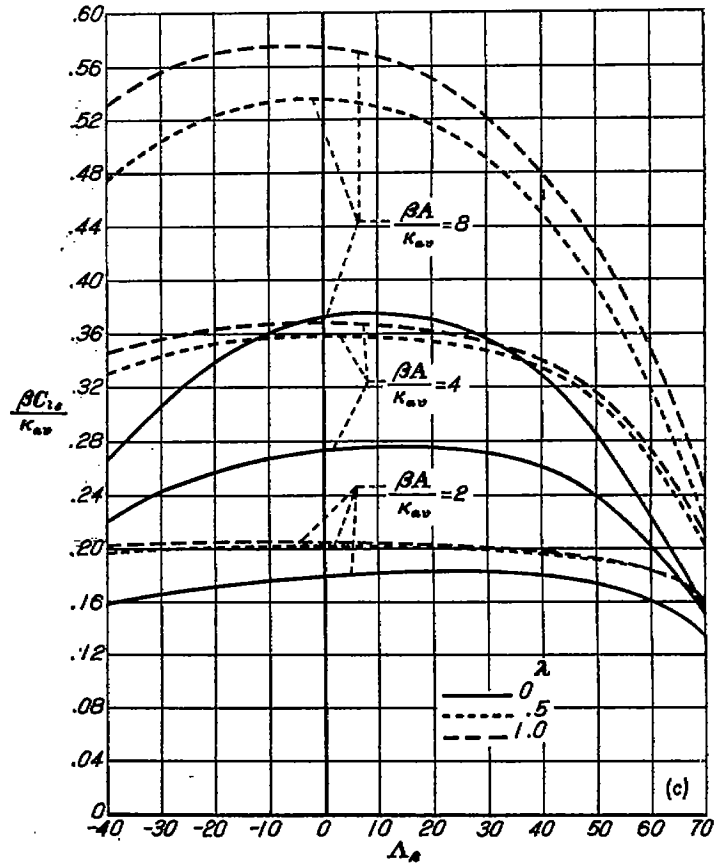

(c) Effect of sweep, $\eta_a=0.5$.

FIGURE 12.—Concluded.

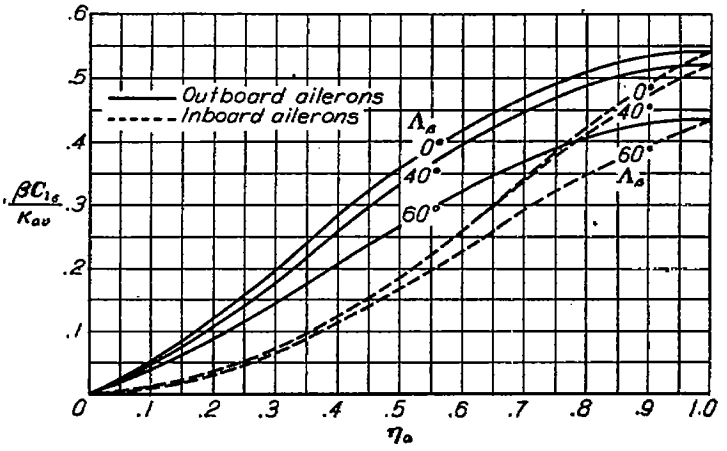

FIGURE 13.—Aileron rolling-moment parameter $\frac{\beta C_{l_\xi}}{\kappa_{av}}$, per radian, for $\frac{\beta A}{\kappa_{av}}=4$, $\lambda=0.5$, as a function of outboard and inboard aileron spans.

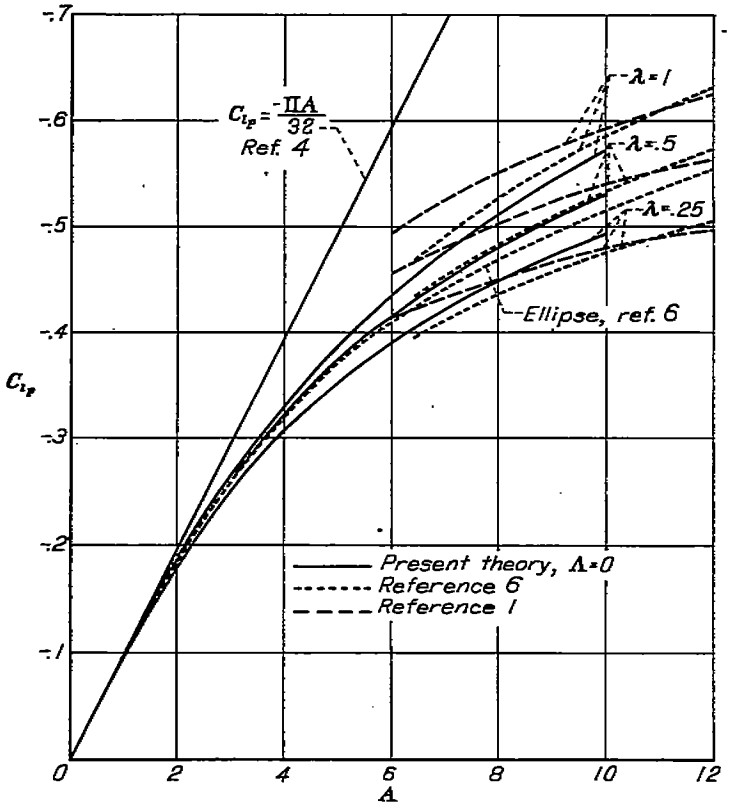

FIGURE 14.—Comparison of damping-in-roll coefficient C_{l_p} of the present theory with those of the theories of references 1, 4, and 6.

The loading distributions due to rolling as given by the present theory are compared in figure 16 with low-speed experimental results for a range of swept wings. The sweep angle seems to have considerably more influence on loading distribution as given by experiment than the theory indicates. The experimental pressure data, however, were very erratic and no firm conclusion can be made.

Experimental values of rolling effectiveness due to aileron deflection are compared with theoretically predicted values in a correlation diagram given by figure 17. Included are the results of a wide range of plan forms which do not vary consistently with any geometric parameter or aileron configuration. Sketches of the plan forms and ailerons are drawn about the points of correlation. The theory makes use of the curve of figure 3 giving $d\alpha/d\delta$ for a sealed-gap aileron over a range of deflection of $\pm 10°$. Experimental results for aileron deflections greater than 15° measured perpendicular to the hinge line were not included. The correlation points of figure 17 scatter appreciably; however, the mean line of the points does approximate the line of perfect correlation.

Figure 17 does not account for effective plan-form change due to $d\alpha/d\delta$. Only the effectiveness of the low-aspect-ratio triangular wing of figure 17 is exceedingly in error, which is the result of neglecting plan-form change.

The plan-form change due to $d\alpha/d\delta$ can, in part, be considered analogous to that due to section lift-curve-slope change. Thus, the total section lift of a wing, the chord of which is reduced by $d\alpha/d\delta$ and which is at an angle of attack δ, is equal to the lift of the wing-aileron section for which the aileron only is deflected at the angle δ. This change in plan form, unlike the section lift-curve-slope change for which the chordwise loading remains constant, does not account for a large change in chordwise loading. If the lifting line is considered to be at the chordwise center of pressure, then, for partial-wing-span ailerons, the lifting line is in effect broken at the aileron spanwise end and the present theory becomes invalid. For the case of full-wing-span ailerons, the lifting line in effect remains unbroken and lies along the center of chordwise pressure. For this case the wing chord can be reduced by $d\alpha/d\delta$ to account for plan-form change; however, although in the limit of zero aspect ratio the results are the same as those of reference 4, this procedure does not with sufficient accuracy account for the chordwise loading shifting aft at intermediate aspect ratios. For control surfaces, the effective plan-form change due to $d\alpha/d\delta$ is appreciable for the low-aspect-ratio wings such that in the limit of zero aspect ratio the spanwise loading is independent of the ratio of aileron chord to wing chord (reference 4). However, for moderate aspect ratios, $d\alpha/d\delta$ can be used without accounting for plan-form changes as comparison with experiment indicates.

Experimental values of C_{l_β}/Γ are not compared with the present theory since reference 3 gives ample support of the theory.

CONCLUDING REMARKS

The determination of antisymmetric loading for arbitrary wings is shown to be easily obtained by the solution of three simultaneous equations. The coefficients of the simultaneous equations are presented in charts of parameters that include wing geometry, compressibility, and section lift-curve slope as arbitrary quantities. Thus the loading for an arbitrary antisymmetric angle-of-attack distribution can be simply found once the angle-of-attack distribution is chosen.

For the important cases of antisymmetric loading, roll, and aileron deflection, the angle-of-attack distribution is given and the simultaneous equations are formed. Loading for these cases can be found by simply obtaining from charts the coefficients corresponding to the wing geometry, Mach number, and lift-curve slope, inserting in the appropriate equations and solving.

Integration formulas for the loading distributions are given which enable the aerodynamic coefficients C_{l_p} and C_{l_β} to be found. The rolling moment due to sideslip of a wing with dihedral is shown to be equivalent to that of aileron deflection and a procedure for determining its value is given.

For the special case of straight-tapered wings, the loading distributions and values of C_{l_p} and C_{l_β} are given in the chart form for a range of wing plan forms.

Experimental and theoretical verification of the theory is shown to be good. The theory is applicable for large aerodynamic angles, provided the flow remains unseparated. The compressibility considerations are reliable to the speed of sound subject to the limitations of the linearized compressible-flow equation.

AMES AERONAUTICAL LABORATORY,
NATIONAL ADVISORY COMMITTEE FOR AERONAUTICS,
MOFFETT FIELD, CALIF., *December 22, 1949.*

FIGURE 15.—Correlation of theoretical and low-speed experimental damping-in-roll coefficient C_{l_p} for various plan forms.

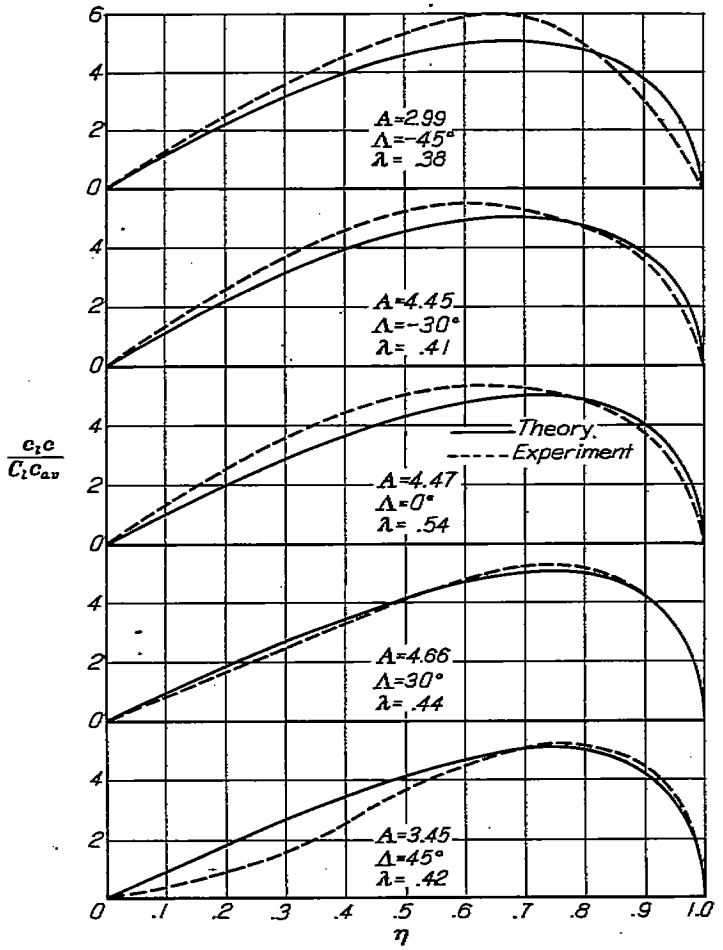

FIGURE 16.—Comparisons of theoretical and low-speed experimental spanwise loading coefficients $\frac{cc}{C_l c_{av}}$ due to rolling of various swept wings.

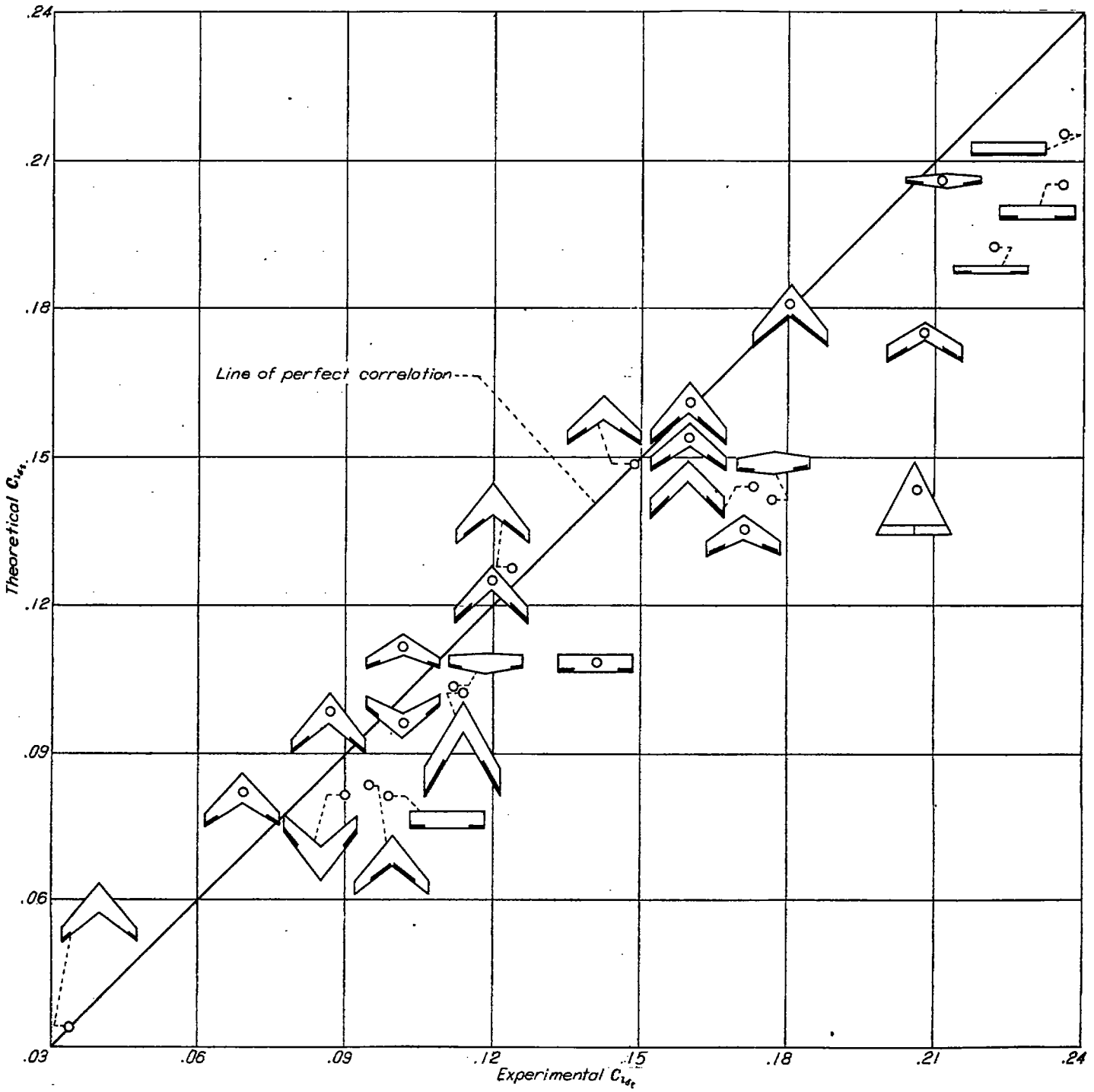

FIGURE 17.—Correlation of theoretical and low-speed experimental aileron-effectiveness $C_{l_{\delta_a}}$ per radian, due to two antisymmetrically deflected ailerons, for various plan forms.

APPENDIX A

EQUATIONS FOR THE DETERMINATION OF ANTISYMMETRIC LOADING

UNSYMMETRIC LOADING

From NACA Rep. 921 (reference 2), the aerodynamic loading is obtained by solution of linear simultaneous equations

$$\alpha_\nu=\left(\frac{w}{V}\right)_\nu=\sum_{n=1}^{m} A_{\nu n}G_n, \qquad \nu=1, 2, \ldots m \tag{A1}$$

where

$$G=\frac{\Gamma_c}{bV} \tag{A2}$$

$$\left.\begin{aligned} A_{\nu n}&=2b_{\nu\nu}+\left(\frac{b}{c_\nu}\right)g_{\nu\nu} \text{ for } n=\nu \\ &=-2b_{\nu n}+\left(\frac{b}{c_\nu}\right)g_{\nu n} \text{ for } n\neq\nu \end{aligned}\right\} \tag{A3}$$

$b_{\nu\nu}$ and $b_{\nu n}$ are coefficients independent of plan form.

$$g_{\nu n}=\frac{-1}{2(M+1)}\left[\frac{L(\nu, 0)f_{n0}+L(\nu, M+1)f_{n,M+1}}{2}+\sum_{\mu=1}^{M} L(\nu, \mu)f_{n\mu}\right] \tag{A4}$$

where

$f_{n\mu}$ are coefficients independent of plan form.

The $L\ (\nu, \mu)$ functions, which can have η_ν negative to find unsymmetrical loading, are given by

for $\bar{\eta}_\mu\geq 0$ or $\mu\leq\frac{M+1}{2}$

$$L(\nu, \mu)=\left\{\frac{\sqrt{\left[1+\left(\frac{b}{c_\nu}\right)\tan\Lambda\left(|\eta_\nu|-\bar{\eta}_\mu\right)\right]^2+\left(\frac{b}{c_\nu}\right)^2(\eta_\nu-\bar{\eta}_\mu)^2}}{1+\left(\frac{b}{c_\nu}\right)(|\eta_\nu|-\eta_\nu)\tan\Lambda}-1\right\}\frac{1}{\left(\frac{b}{c_\nu}\right)(\eta_\nu-\bar{\eta}_\mu)}$$

and

or $\bar{\eta}_\mu\leq 0$ or $\mu\geq\frac{M+1}{2}$

$$L(\nu, \mu)=\left\{\frac{\sqrt{\left[1+\left(\frac{b}{c_\nu}\right)\tan\Lambda\left(|\eta_\nu|+\bar{\eta}_\mu\right)\right]^2+\left(\frac{b}{c_\nu}\right)^2(\eta_\nu-\bar{\eta}_\mu)^2}}{1+\left(\frac{b}{c_\nu}\right)(|\eta_\nu|+\eta_\nu)\tan\Lambda}-1\right\}\frac{1}{\left(\frac{b}{c_\nu}\right)(\eta_\nu-\bar{\eta}_\mu)}+\frac{2\tan\Lambda\sqrt{\left[1+|\eta_\nu|\left(\frac{b}{c_\nu}\right)\tan\Lambda\right]^2+\left(\frac{b}{c_\nu}\right)^2\eta_\nu^2}}{\left[1+\left(\frac{b}{c_\nu}\right)(|\eta_\nu|-\eta_\nu)\tan\Lambda\right]\left[1+\left(\frac{b}{c_\nu}\right)(|\eta_\nu|+\eta_\nu)\tan\Lambda\right]} \tag{A5}$$

where

$\eta_\nu=\cos\frac{\nu\pi}{m+1}$ spanwise position at which downwash is computed

$\bar{\eta}_\mu=\cos\frac{\mu\pi}{M+1}$ spanwise position of incremental loading at the one-quarter-chord line.

The above equations involve computations over the entire wing. However, if the loading is assumed to be symmetric or antisymmetric, the computations can be reduced to less than half the work. The case of symmetric loading is developed in reference 2 and the antisymmetric case is developed in the following section.

ANTISYMMETRIC LOADING

For antisymmetric loading, the loading on each side of the wing has the same magnitude and distribution but with opposite sign, or

$$\left.\begin{aligned} \alpha_\nu&=-\alpha_{m+1-\nu} \\ G_\nu&=-G_{m+1-\nu}, \text{ or } G_n=-G_{m+1-n} \end{aligned}\right\} \tag{A6}$$

Equation (A1) can then be written as

$$\alpha_\nu=\sum_{n=1}^{\frac{m-1}{2}}(A_{\nu n}-A_{\nu, m+1-n})G_n \tag{A7}$$

where the summation is only to $\frac{m-1}{2}$, since $G_{\frac{m+1}{2}}=0$ for antisymmetric loading.

With equations (A3), equation (A7) becomes

$$\alpha_\nu=\left[2(b_{\nu\nu}-b_{\nu, m+1-\nu})+\left(\frac{b}{c_\nu}\right)(g_{\nu\nu}-g_{\nu, m+1-\nu})\right]G_\nu-\sum_{n=1}^{\frac{m-1}{2}}{}'\left[2(b_{\nu n}-b_{\nu, m+1-n})-\left(\frac{b}{c_\nu}\right)(g_{\nu n}-g_{\nu, m+1-n})\right]G_n \tag{A8}$$

(The prime indicates the value for $n=\nu$ is not summed.) Now, from equation (A4)

$$g_{\nu n}+g_{\nu,\,m+1-n}=\frac{-1}{2(M+1)}\left[\frac{L(\nu,0)\,(f_{no}-f_{m+1-n,\,o})}{2}+\frac{L(\nu,M+1)\,(f_{n,\,M+1}-f_{m+1-n,\,M+1})}{2}+\sum_{\mu=1}^{M}L(\nu,\mu)\,(f_{n\mu}-f_{m+1-n,\,\mu})\right] \quad \text{(A9)}$$

where

$$f_{n\mu}=\frac{2}{m+1}\sum_{\mu_1=1}^{m}\mu_1 \sin \mu_1\phi_n \cos \mu_1\phi_\mu \quad \text{(A10)}$$

and

$$\phi_n=\frac{n\pi}{m+1},\ \phi_\mu=\frac{\mu\pi}{M+1}$$

From equation (A9), $f_{n\mu}-f_{m+1-n,\,\mu}$ can be defined as

$$f^*_{n\mu}=f_{n\mu}-f_{m+1-n,\,\mu}$$

then, using equation (A10),

$$f^*_{n\mu}=\frac{2}{m+1}\sum_{\mu_1=1}^{m}\mu_1 \cos \mu_1\phi_\mu\,(\sin \mu_1\phi_n-\sin \mu_1\phi_{m+1-n})$$

$$=\frac{2}{m+1}\sum_{\mu_1=1}^{m}\mu_1 \cos \mu_1\phi_\mu \sin \mu_1\phi_n\,(1+\cos \mu_1\pi)$$

and, since the terms of the summation for odd μ_1 vanish,

$$f^*_{n\mu}=\frac{4}{m+1}\sum_{\mu_1=2,\,4,\,6\ldots \text{ even}}^{m}\mu_1 \sin \mu_1\phi_n \cos \mu_1\phi_\mu \quad \text{(A11)}$$

From equation (A11),

$$f^*_{n\mu}=f^*_{n,\,M+1-\mu} \quad \text{(A12)}$$

Combining equation (A9) with (A12) and defining

$$g^*_{\nu n}=g_{\nu n}-g_{\nu,\,m+1-n}$$

then

$$g^*_{\nu n}=\frac{-1}{2(M+1)}\sum_{\mu=0}^{\frac{M+1}{2}}[L(\nu,\mu)+L(\nu,M+1-\mu)]f^*_{n\mu} \quad \text{(A13)}$$

where for $\mu=0$ and $\frac{M+1}{2}$, $f^*_{n\nu}$ is equal to half the values given by equation (A11) in order that the products can be fitted into the summation. With equation (A13), equation (A8) can be written as

$$\alpha_\nu=\left(2C_\nu+\frac{b}{c_\nu}\,g^*_{\nu\nu}\right)G_\nu-\sum_{n=1}^{\frac{m-1}{2}}{}'\left(2C_{\nu n}-\frac{b}{c_\nu}\,g^*_{\nu n}\right)G_n \quad \text{(A14)}$$

$$\nu=1,2,3,\ldots\frac{m-1}{2}$$

where

$$C_\nu=b_{\nu\nu}-b_{\nu,\,m+1-\nu}$$

$$C_{\nu n}=b_{\nu n}-b_{\nu,\,m+1-n}$$

From reference 2,

$$b_{\nu n}=\frac{\sin \phi_n}{(\cos \phi_n-\cos \phi_\nu)^2}\left[\frac{1-(-1)^{n-\nu}}{2(m+1)}\right]$$

which gives zero values for $b_{\nu n}$ for even $(n-\nu)$ values. Then, since m is odd,

$$b_{\nu,\,m+1-\nu}=0$$

and

$$C_\nu=b_{\nu\nu}$$

It should be noted that $L(\nu,\mu)$ simplifies somewhat for the antisymmetrically loaded wing since η now is only positive in equation (A5). If only positive values of $\bar{\eta}$ are used, then equation (A5) can be written as

$$L^*(\nu,\mu)=L^*_{\nu\mu}=L(\eta,\bar{\eta})+L(\eta,-\bar{\eta})$$

$$=L(\nu,\mu)+L(\nu,M+1-\mu)$$

In summary, the foregoing analysis for the antisymmetrically loaded wing gives

$$\alpha_\nu=\sum_{n=1}^{\frac{m-1}{2}}p_{\nu n}G_n \quad \text{(A15)}$$

$$\nu=1,2,3,\ldots\frac{m-1}{2}$$

where

$$p_{\nu n}=2b_{\nu\nu}+\frac{b}{c_\nu}\,g^*_{\nu\nu} \text{ for } n=\nu \quad \text{(A16)}$$

$$=-2C_{\nu n}+\frac{b}{c_\nu}\,g^*_{\nu n} \text{ for } n\neq\nu$$

$$C_{\nu n}=b_{\nu n}-b_{\nu,\,m+1-n}$$

$$b_{\nu\nu}=\frac{m+1}{4\sin \phi_\nu}$$

$$b_{\nu n}=\frac{\sin \phi_n}{(\cos \phi_n-\cos \phi_\nu)^2}\left[\frac{1-(-1)^{n-\nu}}{2(m+1)}\right]$$

$$g^*_{\nu\nu}=g^*_{\nu n} \text{ for } n=\nu$$

$$g^*_{\nu n}=-\frac{1}{2(M+1)}\sum_{\mu=0}^{\frac{M+1}{2}}L^*_{\nu n}f^*_{n\mu}$$

$$f^*_{n\mu}=\frac{4}{m+1}\sum_{\mu_1=\text{even}}^{m}\mu_1 \sin \mu_1\phi_n \cos \mu_1\phi_\mu$$

$$f^*_{no}=\frac{f^*_{n\mu}}{2} \text{ for } \mu=0$$

$$f^*_{n\,\frac{M+1}{2}}=\frac{f^*_{n\mu}}{2} \text{ for } \mu=\frac{M+1}{2}$$

For $M=m$, $f^*_{n\mu}$ simplifies to

$$f^*_{n\mu}=\left[\frac{2(-1)^{n+\mu}\sin 2\phi_n}{\cos 2\phi_n-\cos 2\phi_\mu}\right]_{\mu\neq n}=\left(\frac{-\sin 4\phi_n}{1-\cos 4\phi_n}\right)_{n=\mu}$$

$$f^*_{n0}=\frac{f^*_{nn}}{2} \text{ for } \mu=0$$

$$f^*_{n\,\frac{m+1}{2}}=\frac{f^*_{n\mu}}{2} \text{ for } \mu=\frac{m+1}{2}$$

$$L^*_{\nu\mu}=\frac{1}{\left(\frac{b}{c_\nu}\right)(\eta_\nu-\bar{\eta}_\mu)}\left\{\sqrt{\left[1+\left(\frac{b}{c_\nu}\right)(\eta_\nu-\bar{\eta}_\mu)\tan\Lambda\right]^2+\left(\frac{b}{c_\nu}\right)^2(\eta_\nu-\bar{\eta}_\mu)^2}-1\right\}+\frac{1}{\left(\frac{b}{c_\nu}\right)(\eta_\nu+\bar{\eta}_\mu)}\left\{\frac{\sqrt{\left[1+\left(\frac{b}{c_\nu}\right)(\eta_\nu-\bar{\eta}_\mu)\tan\Lambda\right]^2+\left(\frac{b}{c_\nu}\right)^2(\eta_\nu+\bar{\eta}_\mu)^2}}{1+2\left(\frac{b}{c_\nu}\right)\eta_\nu\tan\Lambda}-1\right\}+\frac{2\tan\Lambda\sqrt{\left[1+\left(\frac{b}{c_\nu}\right)\eta_\nu\tan\Lambda\right]^2+\left(\frac{b}{c_\nu}\right)^2\eta_\nu^2}}{1+2\left(\frac{b}{c_\nu}\right)\eta_\nu\tan\Lambda}$$

$\eta_\nu=\cos\phi_\nu$ where $\phi_\nu=\frac{\nu\pi}{m+1}$

$\bar{\eta}_\mu=\cos\phi_\mu$ where $\phi_\mu=\frac{\mu\pi}{M+1}$

$\bar{\eta}_n=\cos\phi_n$ where $\phi_n=\frac{n\pi}{m+1}$

For a discussion of the relative accuracies obtained for a choice of values of M and m, see reference 7. The most favorable application is with $M=m$.

APPENDIX B

DERIVATION OF RELATIONS USED IN THE METHOD

APPLICATION OF APPENDIX A

With appendix A, the antisymmetrical loading on a plan form for any antisymmetrical distribution of α_ν can be found. The principal work in the computations is to obtain the coefficients of the simultaneous equations (A15). These coefficients can be presented in charts for the complete range of geometric plan-form parameters into which are introduced the effects of compressibility and section lift-curve slope. With the loading due to rolling known, the coefficients and derivatives are obtained by integration formulas.

Section lift-curve-slope effect.—For a two-dimensional wing with the loaded line at the quarter-chord position, the position x aft of the loaded line where the induced downwash equals the angle of attack of the wing can be obtained by the Biot Savart Law as

$$w=\frac{\Gamma_c}{2\pi x} \text{ where } \Gamma_c=\frac{c_l c V}{2}$$

or

$$\frac{w}{V}=\frac{c_l c}{4\pi x}=\alpha$$

or

$$\frac{dc_l}{d\alpha}=\frac{4\pi x}{c}$$

then

$$x=\left(\frac{c}{4\pi}\right)\frac{dc_l}{d\alpha}$$

where $dc_l/d\alpha$ is the section lift-curve slope. Two dimensional section compressibility effects that do not follow the Prandtl-Glauert rule can be given consideration by taking the ratio of $(dc_l/d\alpha)_{\text{compressible}}$ at a Mach number to $2\pi/\beta$. Let κ be the ratio of the section lift-curve slope at a given Mach number to $2\pi/\beta$ or $(dc_l/d\alpha)_{\text{compressible}}=2\pi\kappa/\beta$, then

$$x=\kappa(c/2)$$

Then the induced angle, $\kappa(c/2)$ aft of the loaded line, is equal to the angle of attack of the wing. For $\kappa=1$, this is at the three-quarter-chord line. For section lift-curve slope less than 2π, κ is less than one and the downwash is equal to the angle of attack at some point between the one-quarter- and three-quarter-chord line.

To take into account the section lift-curve-slope variation in the present theory, the downwash must be found at a distance $\kappa(c/2)$ aft of the loaded line. From the formulas of the summation in appendix A, b/c_ν should be taken as $b/\kappa_\nu c_\nu$, where κ_ν is the ratio of section lift-curve slope for a given Mach number at span station ν, to $2\pi/\beta$.

Derivation of parameters for $p_{\nu n}$.—The $p_{\nu n}$ coefficients, as defined by equation (A16) in appendix A, depend on plan-form geometry in the $(b/c_\nu)L^*_{\nu n}$ functions only, or $p_{\nu n}$ is a function of b/c_ν and sweep angle. As previously shown, b/c_ν is also a function of the spanwise variation of section lift-curve slope and is effectively equivalent to $b/\kappa_\nu c_\nu$, where κ_ν is the ratio of section lift-curve slope for a given Mach number at span station ν to $2\pi/\beta$. The $p_{\nu n}$ coefficients can be plotted against $b/\kappa_\nu c_\nu$ with sweep angle as a parameter; however, $b/\kappa_\nu c_\nu$ will vary from zero to very large values for a range of plan-form geometry, and the plots become unwieldy. For a range of aspect ratio, the values of $b/\kappa_\nu c_\nu$ are a maximum for the zero tapered wings when $\eta_\nu \geq 0.5$ (provided plan-form edges are not concave) and a maximum for the inverse-tapered wings for $\eta_\nu \leq 0.5$. The ratio of $b/\kappa_\nu c_\nu$ for $\eta_\nu \geq 0.5$ for any plan form to those of the zero tapered wing or the ratio of $b/\kappa_\nu c_\nu$ for $\eta_\nu \leq 0.5$ for any plan form to those of the inverse-tapered wing gives a geometric parameter for any plan form that has maximum values that depend only on aspect ratio.

The chord distribution for straight-tapered wings is given by

$$\frac{b}{c_\nu}=\frac{A(1+\lambda)}{2[1-|\eta_\nu|(1-\lambda)]} \tag{B1}$$

Then, for $\lambda=0$,

$$\frac{b}{Ac_\nu}=\frac{1}{2(1-|\eta_\nu|)} \tag{B2}$$

and for $\lambda=1.5$

$$\frac{b}{Ac_\nu}=\frac{5}{2(2+|\eta_\nu|)} \tag{B3}$$

The ratio of $b/\kappa_\nu c_\nu$ to equations (B2) and (B3) gives, respectively, a geometric parameter as

$$\left.\begin{aligned}\frac{b/\kappa_\nu c_\nu}{(b/Ac_\nu)_{\lambda=0}}&=2(1-\eta_\nu)\left(\frac{b}{\kappa_\nu c_\nu}\right) \text{ for } 0.5\leq\eta_\nu<1\\ \frac{b/\kappa_\nu c_\nu}{(b/Ac_\nu)_{\lambda=1.5}}&=\frac{2(2+\eta_\nu)}{5}\left(\frac{b}{\kappa_\nu c_\nu}\right) \text{ for } 0\leq\eta_\nu\leq 0.5\end{aligned}\right\} \tag{B4}$$

Let H_ν be defined as two-fifths times the values of equation (B4) (the fraction two-fifths is introduced to give H_ν the approximate values of $p_{\nu n}$ to simplify plotting procedures), then adding effects of compressibility (see Discussion section)

$$H_\nu=d_\nu\left(\frac{\beta b}{\kappa_\nu c_\nu}\right) \tag{B5}$$

where

$$d_\nu=\frac{4(1-\eta_\nu)}{5} \text{ for } 0.5\leq\eta_\nu<1$$

$$=\frac{4(2+\eta_\nu)}{25} \text{ for } 0\leq\eta_\nu\leq 0.5$$

For tapered wings, H_r simplifies to

$$\left.\begin{aligned} H_r&=\frac{2(1-\eta_r)(1+\lambda)}{5[1-\eta_r(1-\lambda)]}\left(\frac{\beta A}{\kappa_r}\right) \text{ for } 0.5\leq\eta_r<1\\ &=\frac{2(2+\eta_r)(1+\lambda)}{25[1-\eta_r(1-\lambda)]}\left(\frac{\beta A}{\kappa_r}\right) \text{ for } 0\leq\eta_r\leq 0.5\end{aligned}\right\} \quad \text{(B6)}$$

Plots of p_{rn} against H_r in the range of $H_r=0$ to 4 will give p_{rn} coefficients for wings of any chord distribution for aspect ratios up to 10 or 12.

Linear asymptotes of p_{rn}.—For large values of H_r, the p_{rn} functions become linearly proportional to H_r. Since this linear characteristic appears at relatively low values of H_r, the simple linear relation between p_{rn} and H_r is quite usable.

The L^*_{rn} function of appendix A is multiplied by b/c_r and the product is linearized.

$$\left.\begin{aligned}\left(\frac{b}{c_r}\right)L^*_{r\mu}&=\frac{2}{\cos\Lambda}\left(\frac{b}{c_r}\right)-\frac{2\eta}{\eta^2-\bar{\eta}^2}+\left(\frac{1}{|\eta-\bar{\eta}|}+\frac{1}{\eta}\right)\sin\Lambda-\\ &\quad\frac{1}{2\eta}\tan\frac{\Lambda}{2}-\\ &\quad\frac{1}{2\eta}\left[\frac{1-\sqrt{1+\left(\frac{\eta-\bar{\eta}}{\eta+\bar{\eta}}\tan\Lambda\right)^2}}{\tan\Lambda}\right]\ldots\text{for }\bar{\eta}<\eta\\ &=\frac{-2\eta}{\eta^2-\bar{\eta}^2}+\left(\frac{1}{|\eta-\bar{\eta}|}+\frac{1}{\eta}\right)\sin\Lambda-\frac{1}{2\eta}\tan\frac{\Lambda}{2}-\\ &\quad\frac{1}{2\eta}\left[\frac{1-\sqrt{1+\left(\frac{\eta-\bar{\eta}}{\eta+\bar{\eta}}\tan\Lambda\right)^2}}{\tan\Lambda}\right]\ldots\text{for }\bar{\eta}>\eta\\ &=\left(\frac{1}{\cos\Lambda}+\tan\Lambda\right)\left(\frac{b}{c_r}\right)-\frac{1}{2\eta}+\frac{1}{\eta}\sin\Lambda-\\ &\quad\frac{1}{2\eta}\tan\frac{\Lambda}{2}\ldots\text{for }\bar{\eta}=\eta\\ &=\frac{2}{\cos\Lambda}\left(\frac{b}{c_r}\right)-\frac{2}{\eta}+\frac{2\sin\Lambda}{\eta}\ldots\text{for }\bar{\eta}=0\end{aligned}\right\} \quad \text{(B7)}$$

With the values of equation (B7) substituted into equation (A16) the values of p_{rn} for arbitrary sweep angle are obtained. Thus, for $m=7$, the following equation (B8) gives values for p_{rn} as

$$p_{11}=\left(\frac{3.928}{\cos\Lambda}+1.026\tan\Lambda\right)H_1+7.968-1.494\sin\Lambda+$$
$$0.014\tan\frac{\Lambda}{2}+0.082\left(\frac{1-\sqrt{1+0.0016\tan^2\Lambda}}{\tan\Lambda}\right)-$$
$$0.068\left(\frac{1-\sqrt{1+0.0177\tan^2\Lambda}}{\tan\Lambda}\right)+$$
$$0.034\left(\frac{1-\sqrt{1+0.1717\tan^2\Lambda}}{\tan\Lambda}\right)$$

$$p_{12}=\left(\frac{0.851}{\cos\Lambda}-2.901\tan\Lambda\right)H_1-3.138+1.080\sin\Lambda-$$
$$0.034\tan\frac{\Lambda}{2}-0.034\left(\frac{1-\sqrt{1+0.0016\tan^2\Lambda}}{\tan\Lambda}\right)-$$
$$0.096\left(\frac{1-\sqrt{1+0.1717\tan^2\Lambda}}{\tan\Lambda}\right)$$

$$p_{13}=\left(\frac{-0.176}{\cos\Lambda}+1.026\tan\Lambda\right)H_1+0.129-0.869\sin\Lambda+$$
$$0.082\tan\frac{\Lambda}{2}+0.014\left(\frac{1-\sqrt{1+0.0016\tan^2\Lambda}}{\tan\Lambda}\right)+$$
$$0.068\left(\frac{1-\sqrt{1+0.0177\tan^2\Lambda}}{\tan\Lambda}\right)+$$
$$0.034\left(\frac{1-\sqrt{1+0.1717\tan^2\Lambda}}{\tan\Lambda}\right)$$

$$p_{21}=\left(\frac{0.221}{\cos\Lambda}+0.534\tan\Lambda\right)H_2-2.088-0.383\sin\Lambda-$$
$$0.018\tan\frac{\Lambda}{2}-0.088\left(\frac{1-\sqrt{1+0.0177\tan^2\Lambda}}{\tan\Lambda}\right)-$$
$$0.044\left(\frac{1-\sqrt{1+0.0294\tan^2\Lambda}}{\tan\Lambda}\right)-$$
$$0.037\left(\frac{1-\sqrt{1+0.0886\tan^2\Lambda}}{\tan\Lambda}\right)$$

$$p_{22}=\frac{0.975}{\cos\Lambda}H_2+4.596-0.146\sin\Lambda-0.044\tan\frac{\Lambda}{2}+$$
$$0.125\left(\frac{1-\sqrt{1+0.0177\tan^2\Lambda}}{\tan\Lambda}\right)-$$
$$0.044\left(\frac{1-\sqrt{1+0.0294\tan^2\Lambda}}{\tan\Lambda}\right)-$$
$$0.125\left(\frac{1-\sqrt{1+0.0886\tan^2\Lambda}}{\tan\Lambda}\right)$$

$$p_{23}=\left(\frac{0.221}{\cos\Lambda}-0.534\tan\Lambda\right)H_2-1.912+0.221\sin\Lambda+$$
$$0.107\tan\frac{\Lambda}{2}-0.044\left(\frac{1-\sqrt{1+0.0177\tan^2\Lambda}}{\tan\Lambda}\right)+$$
$$0.018\left(\frac{1-\sqrt{1+0.0294\tan^2\Lambda}}{\tan\Lambda}\right)+$$
$$0.044\left(\frac{1-\sqrt{1+0.0886\tan^2\Lambda}}{\tan\Lambda}\right)$$

$$p_{31}=\left(\frac{-0.028}{\cos\Lambda}-0.164\tan\Lambda\right)H_3+0.149+0.324\sin\Lambda+$$
$$0.034\tan\frac{\Lambda}{2}-0.082\left(\frac{1-\sqrt{1+0.1717\tan^2\Lambda}}{\tan\Lambda}\right)-$$
$$0.163\left(\frac{1-\sqrt{1+0.0886\tan^2\Lambda}}{\tan\Lambda}\right)+$$
$$0.197\left(\frac{1-\sqrt{1+0.1993\tan^2\Lambda}}{\tan\Lambda}\right)$$

$$p_{32}=\left(\frac{0.136}{\cos\Lambda}+0.464\tan\Lambda\right)H_3-1.570-0.389\sin\Lambda-$$

$$0.082\tan\frac{\Lambda}{2}+0.231\left(\frac{1-\sqrt{1+0.1717\tan^2\Lambda}}{\tan\Lambda}\right)-0.082\left(\frac{1-\sqrt{1+0.1993\tan^2\Lambda}}{\tan\Lambda}\right)$$

$$p_{33}=\left(\frac{0.628}{\cos\Lambda}-0.164\tan\Lambda\right)H_3+3.417+0.083\sin\Lambda+0.197\tan\frac{\Lambda}{2}-0.082\left(\frac{1-\sqrt{1+0.1717\tan^2\Lambda}}{\tan\Lambda}\right)+0.163\left(\frac{1-\sqrt{1+0.0886\tan^2\Lambda}}{\tan\Lambda}\right)+0.034\left(\frac{1-\sqrt{1+0.1993\tan^2\Lambda}}{\tan\Lambda}\right) \quad \text{(B8)}$$

Linear spanwise distribution of $(\kappa c)_\nu/(\kappa c)_{av}$.—With the condition that the product of section lift-curve slope and wing chord varies linearly spanwise, then

$$\kappa c=\frac{2b}{A_s[1+(\kappa_T/\kappa_R)\lambda]}\{1-\eta_\nu[1-(\kappa_T/\kappa_R)\lambda]\}$$

and equation (3) becomes

$$H_\nu=d_\nu(\beta A_s)\frac{1+(\kappa_T/\kappa_R)\lambda}{2\{1-\eta_\nu[1-(\kappa_T/\kappa_R)\lambda]\}} \quad \text{(B9)}$$

where A_s is the aspect ratio based on the wing chord equal to κc. In equation (B9), H_ν is reduced to terms of two parameters. Expressions of A_s in terms of aspect ratio for straight-tapered wings and the distribution of section lift-curve slope can be found.

For straight-tapered wings

$$A=\frac{2b}{c_R(1+\lambda)}$$

and since κc is linear

$$A_s=\frac{2b}{\kappa_R c_R[1+(\kappa_T/\kappa_R)\lambda]}$$

then

$$A_s=\frac{A}{(\kappa_R+\kappa_T\lambda)/1+\lambda}$$

and equation (B9) becomes

$$H_\nu=d_\nu\left[\frac{\beta A}{(\kappa_R+\kappa_T\lambda)/1+\lambda}\right]\frac{1+(\kappa_T/\kappa_R)\lambda}{2\{1-\eta_\nu[1-(\kappa_T/\kappa_R)\lambda]\}} \quad \text{(B10)}$$

The distribution of κ for straight-tapered wings is given by

$$\kappa_\nu=\frac{(\kappa c)_\nu}{c_\nu}=\kappa_R\frac{1-\eta_\nu[1-(\kappa_T/\kappa_R)\lambda]}{1-\eta_\nu(1-\lambda)} \quad \text{(B11)}$$

Equation (B10) is in terms of two parameters given by $\left[\frac{\beta A}{(\kappa_R+\kappa_T\lambda)/1+\lambda}\right]$ and $(\kappa_T/\kappa_R)\lambda$. Solutions for spanwise loading in terms of these two parameters and Λ_β are valid for the distribution of section lift-curve slope given by equation (B11). Equation (B11) indicates that at $\lambda=1$, κ_ν is a linear function and at $\lambda=0$, κ_ν is a constant. For values of λ between 0 and 1, κ_ν is a curve in the region between the linear function and a constant.

Equation (B10) is given by figure 2 for $m=7$, but with the ordinate given by the parameter $\frac{H_\nu}{\beta A/[(\kappa_R+\kappa_T\lambda)/(1+\lambda)]}$ and the abscissa by $(\kappa_T/\kappa_R)\lambda$.

For the case of linear distribution of $(\kappa c)_\nu$ and straight-tapered wings for which the chord and section lift-curve slope can be specified in three parameters, the loading and associated aerodynamic characteristics can be presented for a range of the parameters Λ_β, $\beta A/[(\kappa_R+\kappa_T\lambda)/(1+\lambda)]$, and $(\kappa_T/\kappa_R)\lambda$.

INTEGRATION OF ANTISYMMETRIC LOADING

Rolling-moment coefficient and derivatives.—Rolling-moment coefficient is given by

$$\beta C_l=\frac{\beta A}{2}\int_{-1}^{1}G(\bar\eta)\bar\eta\,d\bar\eta \quad \text{(B12)}$$

where

$$\bar\eta=\cos\phi$$

which, by an integration formula,

$$\int_{-1}^{1}f(\bar\eta)\,d\bar\eta=\frac{\pi}{m+1}\sum_{n=1}^{m}f(\bar\eta_n)\sin\phi_n \quad \text{(B13)}$$

becomes

$$\beta C_l=\frac{\pi\beta A}{2(m+1)}\sum_{n=1}^{m}G_n\cos\phi_n\sin\phi_n$$

$$=\frac{\pi\beta A}{4(m+1)}\sum_{n=1}^{m}G_n\sin 2\phi_n$$

Since the loading is antisymmetric, $\frac{G_{m+1}}{2}=0$, and

$$\beta C_l=\frac{\pi\beta A}{2(m+1)}\sum_{n=1}^{\frac{m-1}{2}}G_n\sin 2\phi_n \quad \text{(B14)}$$

For spanwise loading due to rolling, the loading is found as a function of $pb/2V$, then equation (B14) divided by $pb/2V$ gives

$$\beta C_{l_p}=\frac{\pi\beta A}{2(m+1)}\sum_{n=1}^{\frac{m-1}{2}}\bar G_n\sin 2\phi_n \quad \text{(B15)}$$

where

$$\bar G=G/(pb/2V)$$

The rolling moment due to ailerons will be found in appendix C.

Induced drag.—The induced drag coefficient is, with equation (B13), given by

$$\beta C_{D_i}=\beta A\int_{-1}^{1}\alpha_i G\,d\eta=\frac{\pi\beta A}{m+1}\sum_{\nu=1}^{m}G_\nu\alpha_{i_\nu}\sin\phi_\nu$$

where α_{i_ν} is one-half the induced angle of the wing wake given by equation (A14) for $c_\nu=\infty$, then for antisymmetric loading

$$\beta C_{D_i}=\frac{2\pi\beta A}{m+1}\sum_{\nu=1}^{\frac{m-1}{2}}\left(b_{\nu\nu}G_\nu^2-G_\nu\sum_{n=1}^{\frac{m-1}{2}}{}'C_{\nu n}G_n\right)\sin\phi_\nu \quad \text{(B16)}$$

where the prime indicates the value of $n=\nu$ is not summed.

Spanwise center of pressure.—The center of pressure on the wing half panel is given by

$$\eta_{c.p.}=\frac{\int_0^1 G\bar{\eta}\,d\bar{\eta}}{\int_0^1 G\,d\bar{\eta}}$$

The numerator is equal to $\beta C_l/\beta A$. If the Fourier series for loading is assumed,

$G(\phi)=\sum_{\mu_1=\text{even}}^{m} a_{\mu_1}\sin\mu_1\phi$, the denominator becomes

$$\sum_{\mu_1=\text{even}}^{m} a_{\mu_1}\int_0^{\frac{\pi}{2}}=\sin\phi\sin\mu_1\phi\,d\phi\sum_{\mu_1=\text{even}}^{m}-a_{\mu_1}(-1)^{\frac{\mu_1}{2}}\left(\frac{\mu_1}{\mu_1^2-1}\right)$$

then

$$\eta_{c.p.}=\frac{\beta C_l}{-\beta A\sum_{\mu_1=\text{even}}^{m} a_{\mu_1}(-1)^{\frac{\mu_1}{2}}\left(\frac{\mu_1}{\mu_1^2-1}\right)} \tag{B17}$$

where a_{μ_1} are the Fourier coefficients.

Loading-due-to-rolling function and interpolation table.—The Fourier series that approximates the antisymmetric loading with only a few terms is given by

$$G(\phi)=\sum_{\mu_1=\text{even}}^{m} a_{\mu_1}\sin\mu_1\phi \tag{B18}$$

The loading G_n is determined at span positions of $\bar{\eta}=\cos\phi_n$ where $\phi_n=\frac{n\pi}{m+1}$. The a_{μ_1} are given by

$$a_{\mu_1}=\frac{2}{\pi}\int_0^{\pi} G(\phi)\sin\mu_1\phi\,d\phi \tag{B19}$$

With the quadrature formula of equation (B13), equation (B19) becomes, for antisymmetric loading,

$$a_{\mu_1}=\frac{4}{m+1}\sum_{n=1}^{\frac{m-1}{2}} G_n\sin\mu_1\phi_n \tag{B20}$$

For $m=7$, the a_{μ_1} coefficients are equal to (for even μ_1)

$$\left.\begin{aligned} a_2&=\frac{1}{2}\left(\frac{\sqrt{2}}{2}G_1+G_2+\frac{\sqrt{2}}{2}G_3\right)\\ a_4&=\frac{1}{2}(G_1-G_3)\\ a_6&=\frac{1}{2}\left(\frac{\sqrt{2}}{2}G_1-G_2+\frac{\sqrt{2}}{2}G_3\right)\end{aligned}\right\} \tag{B21}$$

Equation (B18) with (B21) can be arranged to give

$$\left.\begin{aligned} G(\phi)=&\frac{1}{2}\left(\frac{\sqrt{2}}{2}\sin 2\phi+\sin 4\phi+\frac{\sqrt{2}}{2}\sin 6\phi\right)G_1+\\ &\frac{1}{2}(\sin 2\phi-\sin 6\phi)G_2+\\ &\frac{1}{2}\left(\frac{\sqrt{2}}{2}\sin 2\phi-\sin 4\phi+\frac{\sqrt{2}}{2}\sin 6\phi\right)G_3\end{aligned}\right\} \tag{B22}$$

With equation (B22) the loading due to rolling can be determined at any span position. Letting $\phi=\phi_k=\frac{k\pi}{8}$ and tabulating the factors of G_n as e_{nk}, an interpolation table may be obtained to determine loading at span station k.

TABLE B1, e_{nk}

[$m=7$]

η_k	0.981	0.831	0.556	0.195
n \ k	1/2	3/2	5/2	7/2
1	0.8155	0.5449	−0.1622	0.1084
2	−.2706	−.6533	.6533	−.2706
3	.1084	−.1622	.5449	.8155

$$G_k=\sum_{n=1}^{3} e_{nk}G_n \tag{B23}$$

Equation (B23) may be used for interpolation of any form of loading coefficient, thus

$$\left(\frac{c_l c}{c_l c_{av}}\right)_k=\sum_{n=1}^{3} e_{nk}\left(\frac{c_l c}{c_l c_{av}}\right)_n \tag{B24}$$

APPENDIX C

DETERMINATION OF ANTISYMMETRIC WING TWIST FOR FINDING SPANWISE LOADING DUE TO AILERON DEFLECTION

WING TWIST FOR A GIVEN AILERON SPAN

The determination of loading for an angle-of-attack distribution that contains a discontinuity by a method which satisfies the boundary conditions at a finite number of points can be made by increasing the number of points until the solutions become sufficiently accurate. For the method as given in appendix A, the number of points that satisfy the boundary conditions is given by m. For the large value of m required for accurate results, the computations become exceedingly laborious; however, a procedure using a moderate value of m can be determined by use of a low-aspect-ratio theory with which a wing twist can be found that duplicates the results of the discontinuous angle-of-attack distribution.

A theoretical but relatively simple method of finding spanwise loading due to inboard and outboard ailerons for wings of low aspect ratio is given by reference 4. In the present theory, as aspect ratio approaches zero, $g^*_{\nu n}$ values of appendix A become zero and the $p_{\nu n}$ coefficients given by equation (A16) become constant or independent of plan-form shape and equal to

$$\left.\begin{aligned} p_{\nu n} &= -2C_{\nu n} \\ p_{\nu\nu} &= 2b_{\nu\nu} \end{aligned}\right\} \tag{C1}$$

These coefficients are given by the relations under equation (A15) and $p_{\nu n}$ can be tabulated.

TABLE C1.—$p_{\nu n}$

[For $m=7$ and $A=0$]

n \ ν	1	2	3
1	10.4524	−2.0000	0
2	−3.6954	5.6568	−1.5308
3	0	−2.0000	4.3296

With equation (A15), antisymmetric loading can be found for zero-aspect-ratio wings. As a comment on the accuracy of the present theory for $m=7$, the solution of equation (A15), with the $A=0$ $p_{\nu n}$ values for loading due to rolling gave the same values at the three semispan stations as does reference 4, namely, $G(\phi)=-\dfrac{(pb/2V)\sin 2\phi}{4}$.

The zero-aspect-ratio theory of reference 4 shows that all span loading characteristics are independent of plan-form shape for zero aspect ratio. This independence makes that theory ideal for obtaining the boundary conditions of the present theory for zero aspect ratio, which should apply with the present theory for higher aspect ratios for which plan-form shape has an effect on spanwise loading. The boundary conditions of the present theory are given by the antisymmetric values of α_ν in equation (A15). The problem is to find what antisymmetrical distribution of α_ν is required for the present theory to duplicate the exact loading distribution given by reference 4 for a given aileron span.

The aileron spans are arbitrarily chosen for the present theory as the mean value of the spanwise trigonometric coordinate of the downwash point at a section angle of attack equal to zero. For $m=7$, three aileron spans can be defined for both outboard and inboard ailerons. Let η_a be the aileron span, and θ the spanwise point of the end of the aileron, then

$$\eta_a = 1-\cos\theta \text{ for outboard ailerons}$$

$$\eta_a = \cos\theta \text{ for inboard ailerons}$$

For the present theory, the aileron spans defined are tabulated as follows:

TABLE C2

	Outboard			Inboard		
Case	I	II	III	IV	V	VI
θ	$\frac{3\pi}{16}$	$\frac{5\pi}{16}$	$\frac{7\pi}{16}$	$\frac{5\pi}{16}$	$\frac{3\pi}{16}$	0
η_a	0.1685	0.4444	0.8049	0.5556	0.8315	1.0000

For the aileron spans listed in table C2, the exact span loading distribution can be found from reference 4. With the $p_{\nu n}$ values listed in table C1 and the exact values of G_1, G_2, and G_3 from reference 4, equation (A15) gives the twist required for the present theory to give the loading distribution for each case listed in table C2 or

$$\left.\begin{aligned} \frac{\alpha_1}{\delta} &= 10.4524\left(\frac{G_1}{\delta}\right)-3.6954\left(\frac{G_2}{\delta}\right) \\ \frac{\alpha_2}{\delta} &= -2\left(\frac{G_1}{\delta}\right)+5.6568\left(\frac{G_2}{\delta}\right)-2\left(\frac{G_3}{\delta}\right) \\ \frac{\alpha_3}{\delta} &= -1.5308\left(\frac{G_2}{\delta}\right)+4.3296\left(\frac{G_3}{\delta}\right) \end{aligned}\right\} \tag{C2}$$

The spanwise loading distribution from reference 4 for outboard ailerons is given by

$$\left[\frac{G(\phi)}{\delta}\right]_{\text{outboard}} = \frac{1}{\pi}\left[(\cos\phi-\cos\theta)\,ln\left|\frac{\sin\frac{\theta+\phi}{2}}{\sin\frac{\theta-\phi}{2}}\right| - (\cos\phi+\cos\theta)\,ln\left|\frac{\cos\frac{\theta+\phi}{2}}{\cos\frac{\theta-\phi}{2}}\right|\right] \tag{C3}$$

For the full-wing-span aileron, $\theta=\frac{\pi}{2}$ or $\eta_a=1$

$$\left[\frac{G(\phi)}{\delta}\right]_{\eta_a=1}=\frac{2}{\pi}\cos\phi ln\left|\frac{1+\sin\phi}{\cos\phi}\right| \tag{C4}$$

For inboard ailerons, with the same value of θ

$$\left[\frac{G(\phi)}{\delta}\right]_{\text{inboard}}=\left[\frac{G(\phi)}{\delta}\right]_{\eta_a=1}-\left[\frac{G(\phi)}{\delta}\right]_{\text{outboard}} \tag{C5}$$

With equations (C3), (C4), and (C5), the spanwise loading G_1, G_2, and G_3 at span stations $\phi=\pi/8$, $\pi/4$, and $3\pi/8$, or $\eta=0.9239$, 0.7071, and 0.3827 can be tabulated for each of the cases given in table C2.

TABLE C3

$\frac{G_n}{\delta}$	Case 1	II	III	IV	V	VI
$\frac{G_1}{\delta}$	0.1136	0.1919	0.2316	0.0454	0.1237	0.2373
$\frac{G_2}{\delta}$	0.0500	.2800	.3851	.1164	.3464	.3964
$\frac{G_3}{\delta}$	.0190	.1022	.3620	.2922	.3754	.3944

The twist distribution required for each case is obtained with equation (C2) and table C3, tabulating

TABLE C4

$\frac{\alpha}{\delta}$	Case I	II	III	IV	V	VI
$\frac{\alpha_1}{\delta}$	1.0029	0.9713	0.9979	0.0444	0.0128	1.0157
$\frac{\alpha_2}{\delta}$	.0174	.9957	.9913	−.0169	.9614	.9788
$\frac{\alpha_3}{\delta}$	.0056	.0139	.9777	1.0868	1.0951	1.1007

With the twist distribution given by table C4, equation (A15) can be used to solve for spanwise loading due to ailerons for any of the six cases.

ROLLING MOMENT DUE TO AILERON DEFLECTION

The rolling moment is given by

$$C_l=\frac{A}{4}\int_0^{\pi}G(\phi)\sin 2\varphi d\phi \tag{C6}$$

For span loading due to ailerons, the loading distribution is distorted sufficiently such that the quadrature formula given by equation (B13) is not sufficiently accurate for $m=7$ to integrate equation (C6). With equation (B18)

$$C_l=\frac{\pi A}{8}a_2 \tag{C7}$$

Expanding equation (B18) for $\varphi=\pi/8$, $\pi/4$, and $3\pi/8$, or obtaining G_1, G_2, and G_3 in series of a's, the sum of the G's gives

$$\frac{2}{a}=\frac{1}{2}(0.7071G_1+G_2+0.7071G_3)+a_{14}-a_{18}+a_{30}-a_{34} \tag{C8}$$

The higher harmonic coefficients can be put as factors of the G_n. The rolling-moment coefficient becomes

$$C_l=A\left\{\frac{0.7071\pi}{16}\left[1+\frac{(a_{14}-a_{18}+a_{30}-a_{34})}{1.2071G_1}\right]G_1+\frac{\pi}{16}\left[1+\frac{(a_{14}-a_{18}+a_{30}-a_{34})}{1.2071G_2}\right]G_2+\frac{0.7071\pi}{16}\left[1+\frac{(a_{14}-a_{18}+a_{30}-a_{34})}{1.2071G_3}\right]G_3\right\} \tag{C9}$$

When h_n is defined as the coefficients of G_n

$$C_l=A(h_1G_1+h_2G_2+h_3G_3) \tag{C10}$$

The ratio of $(a_{14}-a_{18}+a_{30}-a_{34})$ to G_n can be evaluated by the zero-aspect-ratio theory. It is expected this ratio will not vary appreciably with aspect ratio. From reference 4, the loading series expansion gives for equation (B18)

$$\left.\begin{aligned}\left(\frac{a_{\mu_1}}{\delta}\right)_{\text{outboard}}&=\frac{4}{\pi\mu_1(\mu_1^2-1)}(\cos\theta\sin\mu_1\theta-\mu_1\sin\theta\cos\mu_1\theta)\\ \left(\frac{a_{\mu_1}}{\delta}\right)_{\eta_a=1}&=\frac{-(-1)^{\frac{\mu_1}{2}}}{\mu_1^2-1}\\ \left(\frac{a_{\mu_1}}{\delta}\right)_{\text{inboard}}&=\left(\frac{a_{\mu_1}}{\delta}\right)_{\eta_a=1}-\left(\frac{a_{\mu_1}}{\delta}\right)_{\text{outboard}}\end{aligned}\right\} \tag{C11}$$

These high harmonic coefficients are small, but are not negligible for loading due to ailerons. The h_n are tabulated for each of the cases

TABLE C5

h_n	Case I	II	III	IV	V	VI
h_1	0.1398	0.1388	0.1379	0.1462	0.1407	0.1402
h_2	.1994	.1963	.1955	.2004	.1973	.1975
h_3	.1446	.1388	.1382	.1400	.1394	.1397

SPANWISE LOADING DISTRIBUTION

The spanwise loading distributions due to the twist distributions of table C4 are found at three span stations, and, since these loadings are not completely defined by a few terms of the assumed loading series, the values of loading at other span stations cannot be found accurately by direct use of equation (B23) and table B1. For zero-aspect-ratio wings, the spanwise loading distribution due to aileron deflection is given to all span stations by equation (C3). The loading distribution for other than zero-aspect-ratio wings will fluctuate about the value given by equation (C3) in a manner similar to the manner that loading due to rolling varies about the function $\sin 2\phi$ of zero-aspect-ratio theory. Since the interpolation table of equation (B23) applies only to loadings that vary about the function $\sin 2\phi$ the loading due to aileron deflection can be divided by the ratio of equation (C3) to $\sin 2\phi$ and the resulting loading will be approximately given by $\sin 2\phi$.

The zero-aspect-ratio values of equation (C3) can be tabulated as ratios of $\frac{G(\phi)/\delta}{\sin 2\phi}$. Define

$$R_n=\frac{G(\phi_n)/\delta}{\sin 2\phi_n} \tag{C12}$$

The zero-aspect-ratio values of R_n can be tabulated for each aileron-span case considered.

TABLE C6.—R_n

	Outboard			Inboard		
Case	I	II	III	IV	V	VI
n \ η_n	0.1685	0.4444	0.6049	0.5556	0.8315	1.0000
1	0.1607	0.2714	0.3275	0.0642	0.1749	0.3358
2	.0500	.2800	.3851	.1164	.3464	.3964
3	.0269	.1445	.5119	.4132	.5309	.5578

The interpolation series of equation (B23) becomes

$$\left(\frac{\overline{\overline{G}}}{R}\right)_k=\sum_{n=1}^{3} e_{nk}\left(\frac{\overline{\overline{G}}}{R}\right)_n \qquad \text{(C13)}$$

where $\overline{\overline{G}}=\frac{G}{\delta}$ and e_{nk} are given by table B1. With R_k tabulated, values of loading at span stations $\eta_k=\cos\frac{k\pi}{8}$ are obtained.

TABLE C7.—R_k

η_k	Case \ k	I	II	III	IV	V	VI
0.981	1/2	0.1738	0.2663	0.3162	0.0559	0.1484	0.3222
.831	3/2	.1056	.2787	.3499	.0802	.2533	.3589
.556	5/2	.0341	.2250	.4365	.2424	.4225	.4566
.195	7/2	.0233	.1212	.5304	.6363	.7843	.7575

REFERENCES

1. Pearson, Henry A., and Jones, Robert T.: Theoretical Stability and Control Characteristics of Wings With Various Amounts of Taper and Twist. NACA Rep. 635, 1938.
2. DeYoung, John, and Harper, Charles W.: Theoretical Symmetric Span Loading at Subsonic Speeds for Wings Having Arbitrary Plan Form. NACA Rep. 921, 1948. (Formerly NACA TN's 1476, 1491, 1772)
3. Bird, John D.: Some Theoretical Low-Speed Span Loading Characteristics of Swept Wings in Roll and Sideslip. NACA TN 1839, 1949.
4. DeYoung, John: Spanwise Loading for Wings and Control Surfaces of Low Aspect Ratio. NACA TN 2011, 1950.
5. Toll, Thomas A.: Summary of Lateral-Control Research. NACA TN 1245, 1947.
6. Swanson, Robert S., and Priddy, E. LaVerne: Lifting-Surface-Theory Values of the Damping in Roll and of the Parameter Used in Estimating Aileron Stick Forces. NACA ARR L5F23, 1945.
7. Weissinger, J.: The Lift Distribution of Swept-Back Wings. NACA TM 1120, 1947.

TABLE I.—ANTISYMMETRIC INFLUENCE COEFFICIENTS, p_{rs}, BEYOND THE SCOPE OF FIGURE 1

p_{11}

H_1 \ A	−80	−40	−20		20	40	50	60	70	75
0.4										14.22
0.6									15.23	17.99
0.8								14.61	18.05	21.84
1.2	15.15					14.69	15.93	18.36	23.86	29.34
1.6	17.05	15.68	15.01	14.78	15.23	16.91	18.77	22.17	29.81	37.09
2.0	18.89	16.91	16.48	16.25	16.98	19.25	21.62	26.03	35.88	
2.4		19.35	17.93	17.73	18.68	21.00	24.48	30.02		
2.8			19.53	19.26	20.46	23.91	27.32	34.07		
3.2			21.19	20.81	22.27	26.22	30.20	38.24		
3.6				22.42	24.08	28.53				
4.0				24.05	25.86	30.84				

p_{12}

H_1 \ A	−80	−40	−20	0	20	40	50	60	70	75
0.6	−1.17									−5.59
0.8	−.25	−1.11							−6.51	−8.17
1.2	1.70	.26	−1.33					−6.29	−8.71	−9.67
1.6	3.64	1.68	−.52					−7.58	−11.01	−11.18
2.0	3.61	3.12	.28				−6.66	−8.90	−13.23	−14.19
2.4		4.62	1.08	−1.22			−7.50	−10.24	−15.54	
2.8			1.86	−.87			−8.35	−11.57		
3.2			2.61	−.51		−6.70	−9.21	−12.92		
3.6			3.37	−.16		−7.20	−10.09			
4.0				.18		−7.72	−10.95			